The Journal of Headache and Pain

RESEARCH

Open Access

Induction of more severe central sensitization in a medication overuse headache model mice through active ingestion of rizatriptan

Zhenjie Ma[1,2†], Chenhao Li[3†], Wenhao Bai[4], Wei Xie[1,2], Mingjie Zhang[1,2], Han Xiao[1,2], Cancan Chen[1,2], Yang Li[5], Wenwen Zhang[6], Deqi Zhai[1,2], Yingyuan Liu[1,2], Dengfa Zhao[1,2], Wenjing Tang[1,2], Zhao Dong[1,2], Ruozhuo Liu[1,2] and Shengyuan Yu[1,2*]

Abstract

Background Medication overuse headache (MOH) is a secondary headache disorder arising from excessive use of acute analgesics in patients with primary headache. Current animal models that predominantly employ passive drug administration fail to recapitulate the hallmark feature of voluntary medication-seeking behaviour observed clinically. Therefore, we established a novel MOH mouse model with the active ingestion of rizatriptan (RIZ) to better simulate the clinical characteristics of MOH and explore changes in brain activation patterns.

Methods C57BL/6 J mice received intraperitoneal injections of nitroglycerin (NTG, 10 mg/kg) every other day. During the feeding period, they were provided with two bottles—one containing an RIZ solution (0.02 mg/kg) and the other containing deuterium depleted water (DDW)—allowing for voluntary intake. The bottle containing the RIZ solution was marked with a fixed colour indicator at the nozzle. Behavioural assessments included mechanical allodynia (von Frey filaments), anxiety-like behaviours (elevated plus maze, EPM and open field test, OFT), and drug-seeking quantification. Quantitative data from c-Fos immunostaining across 25 specific brain regions were subjected to Z score normalization, followed by three-tiered computational analyses: 1) hierarchical clustering (complete linkage) to characterize activation patterns, 2) Pearson correlation analysis for functional connectivity mapping, and 3) graph-theoretical network analysis (Cytoscape 3.2.1) to identify hub regions and their topological relationships. The small molecule calcitonin gene-related peptide (CGRP) receptor antagonist, rimegepant (100 mg/kg, i.p., 7 injections) was administered during the modelling period, and withdrawal of RIZ and NTG was applied after modelling to observe behavioural and histological changes.

Results Chronic RIZ consumption exacerbated NTG-induced cutaneous allodynia, prolonged central sensitization, and increased anxiety-like behaviour. Rimegepant attenuated allodynia progression, whereas withdrawal of RIZ and NTG normalized pain thresholds. Network analysis identified the prelimbic cortex (PrL) and spinal trigeminal nucleus caudalis (SPVC) as hub nodes. The PrL exhibited extensive functional connectivity with addiction-related

†Zhenjie Ma and Chenhao Li contributed equally to this work.

*Correspondence:
Shengyuan Yu
yusy1963@126.com
Full list of author information is available at the end of the article

regions (the insular cortex, IC and nucleus accumbens), whereas the SPVC showed predominant connections with pain-processing areas.

Conclusion This study pioneers an ethologically valid MOH model that reflects more severe central sensitization and recapitulates active medication-seeking behaviour. PrL-mediated addiction-like-behaviour pathways and SPVC-centred nociceptive processing may play roles in the development of MOH. These findings provide novel neuromodulation targets (PrL, IC, SPVC) for refractory MOH management.

Keywords Medication overuse headache, Calcitonin gene-related peptide, Rimegepant, Hierarchical clustering, Network analysis

Introduction

Medication overuse headache (MOH) represents a secondary headache disorder triggered primarily by excessive use of acute analgesic medications in patients with underlying primary headache conditions (90% of MOH cases occur in individuals with a history of episodic migraine and/or tension-type headache) [1–3]. An increase in headache frequency typically correlates with increased consumption of acute medications. Notably, up to 65% of patients with MOH exhibit dependency-related behaviours [4–6], with most continuing daily analgesic use despite minimal therapeutic efficacy for headache relief. The precise pathogenesis and standardized treatment protocols for MOH remain incompletely understood.

MOH is an extremely complex brain dysfunction disorder with a myriad of influencing factors. Several voxel-based MRI studies of patients with MOH have shown that in the pre-withdrawal phase, these patients present increased grey matter density in the midbrain, striatum, cingulate gyrus, subparietal lobule, and cerebellum, and decreased grey matter density in the orbitofrontal cortex, frontal lobe, insula, and parietal cortex. Withdrawal from pain medication resulted in decreased density in the superior temporal gyrus, midbrain, and cerebellum. Functional magnetic resonance revealed enhanced functional connectivity between the salience network and the reinnervated nucleus [7–11]. The above studies suggest that the process of MOH formation is associated with the activation or inhibition of multiple specific brain regions in the central nervous system (CNS).

Calcitonin gene related peptide (CGRP) is a peptide consisting of 37 amino acids that is expressed mainly in C sensory nerve fibres [12]. These nerve fibres are widely distributed throughout the body and play an important role in sensory conduction. Long-term studies have shown that CGRP is closely related to the development of MOH. Some preclinical studies have shown that chronic exposure to opioids, nonsteroidal anti-inflammatory drugs (NSAIDs), and triptans leads to the upregulation of CGRP in the trigeminal ganglion, triggering potential sensitization [13–15]. Several reliable animal studies have shown that small-molecule CGRP antagonists (e.g., olcegepant) [16] or monoclonal antibodies targeting CGRP receptors (e.g., fremanezumab) [17], by inhibiting the CGRP pathway, prevent pain-like behaviours in rats caused by sumatriptan or opioid sensitization. Unlike sumatriptan (a 5-H1B/1D receptor agonist), sustained exposure to drugs such as fremanezumab and olcegepant did not cause neuroplastic changes in trigeminal sensory afferents, such as increases in CGRP expression and in basal trigeminal nociception, further suggesting that repeated administration of CGRP antagonists does not cause MOH [18, 19]. Several prospective clinical studies on the use of monoclonal antibodies targeting CGRP as well as small molecule CGRP receptor antagonists for the treatment of MOH have demonstrated that interventions targeting CGRP and its receptors can reduce the number of headache days per month and acute pain medication intake in patients with MOH [20–23]. These findings suggest that the development of MOH can be influenced by interference with the CGRP pathway.

CGRP expression in the CNS is very widespread. This expression extends from the brainstem to the cortex and encompasses discrete nuclei and extensive fibre networks [24]. However, it is not clear whether the specific brain regions that produce changes during the pathophysiology of MOH involve alterations in the corresponding CGRP system. We designed a two-phase experiment to explore this phenomenon. Phase 1: We established a mouse model that is more consistent with the developmental process of MOH based on the clinical characteristics of the patients. Using this model, we targeted specific brain regions in the CNS associated with the development of MOH by localizing and quantitatively counting c-Fos positive cells in the whole brain. Phase 2: The most effective way to control the progression of MOH currently is to stop the overuse of medications and administer appropriate preventive treatment. Whether to administer prophylactic treatment at the same time or to wait for the effects of withdrawal treatment is another unresolved issue [5, 25]. Therefore, we investigated behavioural changes and hub brain region activation in model mice

using two intervention approaches: drug withdrawal and rimegepant administration.

Materials and methods

Animals

Female C57BL/6 J mice (8–10 weeks old, 20–30 g body weight; SPF grade, SibeiFu Biotechnology, Beijing) were maintained under standardized conditions (23 ± 2 °C, 55 ± 15% humidity, 12-h light/dark cycle) with free access to a standard mouse maintenance diet (Beijing SibeiFu Biotechnology Co., Ltd.) and water. Sample size estimation was performed using G*Power 3.1.9.7 software, adopting a repeated-measures ANOVA framework with a predefined statistical power of 85%. All experimental protocols complied with the Guidelines for the Management of Laboratory Animals and received formal approval from the Institutional Animal Care and Use Committee at Chinese PLA General Hospital.

MOH model construction and behavioural measurement of drug preference

Mice in the same group were placed in the same cage, with 3 mice per cage. Food was placed inside the cage and two bottles of liquid were placed on top of the cage to prevent the mice from interfering with the measurement of the liquid in the bottles due to ingestion. The pairing of the two bottles of liquid consisted of two bottles of deuterium depleted water (DDW) or one bottle of DDW and one bottle of rizatriptan (RIZ, Yangguang Bio., Beijing, China), depending on the grouping. The clinical dosage of RIZ for acute pain relief in patients with migraine is 5 mg [26]. To better mimic the clinical use of RIZ in patients with MOH, the dose was converted from the human dose using body surface area normalization calculations [27], and the final concentration of RIZ was determined to be 0.02 mg/ml. The solvent for the RIZ solution was DDW. Each bottle contained 60 ml of liquid and was wrapped in tinfoil, and at the mouth of the bottle, the two bottles of water were distinguished by different and fixed colours. Each group of mice received an intraperitoneal injection of nitroglycerin (NTG, 10 mg/kg)/normal saline (NS) at fixed times on Days 0, 2, 4, 6, 8, 10, 12 and 14. Twenty-four mice were randomly assigned to four groups according to the type of fluid ingested and intraperitoneally administered drug. The NTG solution was prepared from a stock solution of 5.0 mg/ml NTG (Beijing Yimin, China) in 30% ethanol, 30% propylene glycol, and water. It was then diluted fivefold with NS to obtain a 1 mg/ml solution [28]. For the behavioural determination of drug preference in mice, the main manifestation was the dose of the drug ingested actively because of pain. Therefore, the consumption of liquid in the two bottles of each cage was measured every 48 h using the weighing method and recorded, and the ratio of drug consumption to drinking water consumption in the same group of mice was used to characterize the drug-dependent behaviour. The liquid in the bottles was replaced after each measurement to ensure that the starting amount in all the bottles was the same before each measurement. Solution weighing and replacement were performed by a dedicated experimenter who did not participate in subsequent experiments, ensuring these experimental procedures complied with the blinded protocol.

Behavioural tests

All the mice were placed in the behavioural testing room 2 h before the behavioural assessments were performed to acclimatize them to the environment. Behavioural tests were conducted between 9:00 AM and 5:00 PM. The behavioural laboratory was sufficiently spacious, quiet, and well ventilated. The behavioural tests were performed by the same experimenter, who was blinded to the experimental groups.

Abnormal skin pain sensitization behaviour

Skin pain sensitivity in the mice was assessed by measuring mechanical pain thresholds at the periorbital area and the hind paw [29, 30]. The pain threshold was measured with calibrated von Frey filaments ranging from 0.008–2.0 g (Aesthesio®, Danmic Global, San Jose, CA, USA). Before formal testing, the mice were placed on the pain threshold testing device for 3 days of acclimation training until their limbs naturally stretched and lay flat on the metal grid surface or the craniofacial pain testing platform. Before each formal test, the mice were placed in the testing device to adapt for 30 min. Animals were only eligible for testing if they met the following behavioural criteria: lying flat on the metal mesh surface (or head pain test platform) with all four limbs naturally extended.

To measure the mechanical hind paw pain threshold, the mice were individually placed in a 10 cm × 7 cm × 16 cm transparent Plexiglas box positioned on a metal mesh rack, which allowed the experimenters to observe the hind paw from below. The filaments were vertically applied to the hind paw; a positive response was defined as hind paw withdrawal or licking.

For head mechanical pain threshold testing, the mice were placed on a 7 cm × 7 cm platform 30 cm above the tabletop, and filaments were vertically applied to the periorbital region [31]; a positive response was defined as head retraction or grooming. The testing platform and periorbital measurement range schematic are shown in Fig. 1A.

Using the up–down method [32], a heavier filament was applied following each negative response, and a lighter filament was applied after each positive response.

After the first breaking point, four additional stimulations were conducted, and both the response pattern and the weight of the final filament were recorded. The 50% withdrawal threshold was calculated using the freely available online algorithm at https://bioapps.shinyapps.io/von_frey_app/ [33]. Measurements were conducted before each NTG or control solvent injection [34]. The mice were randomly assigned to groups by an independent individual. Another experimenter performed both the baseline von Frey test and the subsequent behavioural assessments, remaining blinded to group assignments and relying only on the identification numbers.

Migraine triggers

After the pain thresholds of all four groups of mice had returned to levels not significantly different from those at baseline, the mice were injected with a low dose of nitric oxide donor-sodium nitroprusside (SNP, 0.03 mg/kg) diluted in NS in the flaccid skin of the posterior neck [35]. Pain behaviour was measured continuously at 1, 2, 3, 4, and 5 h after stimulus administration.

Assessment of Anxiety-Like Behaviour

Anxiety and depression are the most common comorbidities of headache disorders. Two methods were selected to assess anxiety-like behaviour in this study [36]. The elevated plus maze (EPM) and the open field apparatus were purchased from Shanghai Xinruan Information Technology Co., Ltd. Behavioural data were recorded using SuperMaze software (Information Technology Co., Ltd., XR-Xmaze, Shanghai, China). The sample size for each test is provided in the figure legends. Each mouse was tested within 2 h after NTG/NS injection on different days. The tests were performed by the same experimenter, who was blinded to the experimental groupings and only knew the animal identification numbers.

EPM test

The plus maze was positioned 60 cm above the ground and consisted of two open arms (35 cm in length, 5 cm in width, 60 lx) and two closed arms (35 cm in length, 5 cm in width, < 5 lx), connected by a central area (5 cm × 5 cm) [37]. During testing, the mice were placed in the central area facing an open arm and allowed to explore freely for 5 min.

Behavioural indices were evaluated by recording the time spent in the open arms, the number of open arm entries, the time spent in the closed arms, and the number of closed arm entries.

Open Field Test (OFT)

The open field apparatus was an open-topped cubic structure (500 mm × 500 mm × 400 mm, 58 lx) [38]. A central zone measuring 250 mm × 250 mm was defined as the central zone, with the remaining area designated the peripheral zone. Each mouse was placed in a corner of the arena, with its head oriented towards the centre, and allowed to explore freely for 5 min.

The following multidimensional behavioural parameters were systematically collected in OFT: residence time in the central zone, freezing time in the central zone, activity distance in the central zone, and number of entries into the central zone [39].

Tissue processing

Two hours after the intraperitoneal injection of NTG or control solvent, the mice were deeply anaesthetized with 1.5% Avertin. They were then successively perfused transcardially with 20 ml of 0.1 M phosphate-buffered saline (PBS) buffer (37 °C) and 20 ml of 0.1 M PBS buffer (4 °C), followed by perfusion with 20 ml of cold 4% paraformaldehyde (PFA) solution [40]. The brain tissues were subsequently fixed in 4% PFA (16 h) and sequentially dehydrated through a graded sucrose series (15% → 30%).

Using a cryostat (Leica 1950 M), 30-μm-thick coronal sections were collected and subjected to antigen blocking (1 h at room temperature) in a solution consisting of 10% normal goat serum and 0.5% Triton X-100 in 0.1 M PBS [31]. The sections were then exposed to c-Fos rabbit primary antibodies (1:1000, Cell Signaling Technology, 2250S, USA) and Neun mouse primary antibodies (1:1000, Proteintech, 66,836–1-Ig- 100 μl, China) overnight at 4 °C. After three 10-min washes with PBS, the sections were incubated with a fluorescent dye-conjugated goat anti-rabbit secondary antibody (1:1000, Abcam, ab150080, USA) and a fluorescent dye-conjugated goat anti-mouse secondary antibody (1:1000, Abcam, ab150113, USA) diluted in antibody buffer for 2 h at room temperature (RT). After additional rinsing with PBS (3 × 10 min), the sections were mounted with an antifade mounting medium containing 4′,6-diamidino-2-phenylindole (DAPI, P0131, Beyotime).

Quantification of c-Fos positive cells and visualization of activation levels in brain regions

The imaging system used in this experiment was the PannoramicScan Il digital slide scanner (3DHISTECH KFT., Hungary). All images were acquired using a 20 × objective lens, and the field of view was z-stacked at a thickness of 3 μm. The images were exported at a resolution of 600 dpi using SlideViewer software, where image processing and counting were also performed. The brightness and contrast of the brain sections were adjusted consistently

across groups. The regions of interest with differential expression were determined based on the Paxinos atlas (3rd edition, mouse brain in stereotaxic coordinates). Three random regions of size 200 μm × 200 μm were subsequently selected within each brain region. These regions were magnified 40 times for counting. Because the depth of specific brain regions varies, the number of sections differs for each region. Therefore, the sample size was not selected based on the number of mice in each group. Four to six sections were selected for each brain region, with 3 or 4 mice used per group. The number of c-Fos + cells in each region were counted separately. Statistical analysis was performed using GraphPad Prism 9 software, employing two-way repeated-measures ANOVA followed by Tukey's multiple comparisons test.

For each group, the mean activation count was projected onto the average brain template, with the Allen Mouse Brain Atlas (CCFv3) serving as a reference, using nibabel 5.3.1 and the Allen Software Development Kit v2.16.2 implemented in Python 3.10.16. The resulting activation map was then visualized using MRIcroGL, with selected sections rendered for further analysis. The raw data are presented in Supplementary Material 2.

Hierarchical clustering

We performed hierarchical clustering analysis to identify coactivation and differential activation modules across three experimental comparisons: 1) NTG + RIZ vs. NTG + DDW, 2) NTG + RIZ vs. NS + DDW, and 3) NTG + RIZ vs. NS + RIZ. This approach revealed functional connectivity networks modulated by NTG and RIZ treatment. Pairwise Euclidean distances were calculated from log-transformed c-Fos density values across 25 brain regions. The brain regions demonstrating the highest similarity (smallest distances) across all three comparisons were iteratively clustered using complete linkage criteria, which maintain cluster homogeneity by defining cluster boundaries through the maximum pairwise distance between members. Optimal cluster numbers for co-functional brain regions were determined through consensus of multiple validation criteria, with the final cluster count selected based on maximum criterion agreement. R packages (Nbclust 3.0.1, ggtree 3.6.2, ggplot2 3.5.1 and aplot 0.2.2) were applied. The original data are presented in Supplementary Material 3.

Network generation and Hub identification

Theoretical graph analysis was performed to evaluate how functional connectivity changed in response to treatment with NTG and RIZ in mice [41]. First, correlation matrices of the three experimental groups were generated by computing Pearson correlation coefficients from the log relative c-Fos densities of the 25 identified brain regions. Changes in functional connectivity between major cerebral subdivisions resulting from NTG and RIZ treatment were quantified through mean correlation analysis. Then, weighted undirected networks were constructed by retaining correlations meeting a significance threshold of $r \geq 0.576$ (two-tailed $p < 0.05$, uncorrected; critical value calculated for $n = 12$). In these networks, nodes represented brain regions, and edges represented significant interregional correlations ($r \geq 0.576$), with edge weights corresponding to correlation coefficients. The nodes in the networks correspond to brain regions, and the correlations above the threshold were considered connections. In addition, hub regions were identified using degree, betweenness, and eigenvector centrality measures to identify potential key brain regions [42]. The degree expresses the immediate influence of a specific brain region and is determined by the number of edges connected to a node. Betweenness centrality reflects how each node facilitates communication or connectivity within the network, measured by the number of shortest paths that pass through a given brain region. Eigenvector centrality assesses the influence of a node within a network by recursively weighting the centrality of its direct connections. This metric prioritizes nodes that establish connections with highly central neighbours, such that elevated eigenvector centrality values signify the amplified systemic influence of a node through its association with well-connected network hubs. The Brain Connectivity Toolbox in MATLAB R2016a (MathWorks Inc) [43] and network visualization using Cytoscape (version 3.2.1) were performed for network analysis and visualization [44]. The origin data and code are presented in Supplementary Material 3.

Rimegepant intervention therapy

To determine an appropriate concentration of rimegepant in our rodent model, we referred to available pharmacokinetic data in humans and rats [45, 46]. Based on the findings of Mulder and colleagues [47], a dose of 100 mg/kg was selected for intraperitoneal injection in our study. According to the instruction manual, rimegepant sulfate (Beijing HVSF United Chemical Materials Co., Ltd.) was dissolved in DMSO and NS to prepare a mixed solution at a concentration of 100 mg/kg. The ratio of DMSO to NS was 1:9. Similarly, the vehicle (VEH) was composed of equal proportions (1:9) of DMSO and NS. The rimegepant t mixture or solvent was administered intraperitoneally 30 min prior to each NTG injection, for a total of 7 injections.

Statistical analysis

For experiments involving multiple groups with two dependent variables, two-way repeated-measures

ANOVA with Tukey's post hoc test was employed. Specific statistical tests applied to individual experiments are detailed in the respective figure legends. The data are presented as the means ± standard errors of the means (SEMs). The standardization and analytical workflow for the immunofluorescence data proceeded as follows: First, raw c-Fos expression values across 25 brain regions were converted to log-transformed density values by dividing experimental group (NTG + RIZ) measurements by baseline values from three control groups (NTG + DDW, NS + DDW, NS + RIZ), followed by natural logarithm transformation. Z scores for the NTG + RIZ group were subsequently generated by normalizing these log-transformed values against the means and standard deviations of the three control groups.

To assess the statistical significance of differences in c-Fos expression between groups, Z scores were compared against a zero-centred null distribution, with multiple comparison corrections implemented via the Benjamini–Hochberg procedure (false discovery rate Q = 5%). Normally distributed data were analysed using one-sample t-tests and one-way ANOVA with Tukey's test, whereas nonnormally distributed data were evaluated via Wilcoxon signed-rank tests and Kruskal–Wallis ANOVA followed by Dunn's test. Positive Z-values indicate higher expression in the NTG + RIZ group than in the control group, whereas negative values denote lower expression.

For correlation analyses, Pearson correlation coefficients (R) were subjected to Fisher's Z-transformation prior to group mean comparisons and statistical testing. All analyses were performed using R 4.4.1 and MATLAB R2016a (MathWorks Inc.).

Results

Continuous administration of RIZ exacerbates NTG-induced cutaneous allodynia

Patients with MOH frequently have a primary underlying headache disorder, typically with a prevalence of migraine or TTH [1, 3]. To better mimic the clinical pathogenesis of MOH we performed repeated intraperitoneal injections of NTG in mice to simulate chronic migraine-like headache. The preference of the mice for RIZ was examined by providing both water and a highly concentrated solution of RIZ to the mice. There is growing evidence that MOH is strongly associated with central sensitization. Cutaneous nociceptive sensitization is present in patients with MOH. Clinically, cutaneous allodynia is considered a clinical marker of central sensitization [48–50]. Compared with patients with episodic migraine, patients with MOH and chronic migraine exhibit a greater incidence of cutaneous allodynia [51]. Therefore, we utilized the von-Frey test to detect changes in basal pain thresholds in the head and hind paw of mice to reflect the mechanical threshold. Twenty-eight mice were subjected to pain threshold and preference assessment, and four mice were excluded because of their low baseline pain thresholds. The final sample size was 6 mice per group. We performed a von-Frey assay on the mice 2 h before each intraperitoneal injection of NTG/NS until D14. During drug withdrawal, we continued to perform behavioural acquisition at fixed times every other day until the pain thresholds of the mice were not significantly different from those at D0 (Fig. 1A). Compared with those of NS + DDW group, the mechanical pain thresholds of the head (two-way repeated-measures ANOVA with Tukey's post hoc test: main group effect: $F(3, 20) = 16.57$, $p < 0.0001$; main time effects: $F(4.185, 83.71) = 14.83$, $p < 0.0001$; interaction between group and time: main group effect: $F(15, 100) = 1.973$, $p = 0.0245$) and hind paw (two-way repeated-measures ANOVA with Tukey's post hoc test: main group effect: $F(3, 20) = 71.50$, $p < 0.0001$; main time effects: $F(5.844, 116.9) = 42.78$, $p < 0.0001$; interaction between group and time: $F(48, 320) = 3.922$, $p < 0.0001$.) in the NTG + DDW, NS + RIZ, and NTG + RIZ groups decreased significantly over time during the modelling period (between D0 and D14), and the mechanical sensitivity persisted for at least 3 weeks after the completion of modelling. At the end of modelling on D14, the NTG + RIZ group presented a lower hind paw mechanical pain threshold than the NS + RIZ group did ($p < 0.01$). During the measurement of the hind paw pain threshold, the mice in the NTG + RIZ group exhibited strong avoidance of the 0.008 g von Frey fibre filaments, which manifested as avoidance behaviour (i.e., mice kept their limbs near the walls of the acrylic box); and the above phenomena did not occur in the remaining three groups. This difference was not significant in the measurement of the head pain threshold, which may be related to the "floor effect", i.e., the pain threshold of the mice was so sensitive that the smallest range of von Frey filaments was unable to discriminate between groups. During drug withdrawal, pain thresholds returned to the D0 level at D30 ($p = 0.2850$) and D28 ($p = 0.3183$) in the NS + RIZ and NTG + DDW groups, respectively. In contrast, the NTG + RIZ group did not return to normal pain thresholds until D40 ($p = 0.1517$) (Fig. 1B). These results suggest that persistent overdose of RIZ exacerbates NTG-induced abnormal skin pain and tends to prolong the pain response.

Repeated NTG interventions increase active RIZ intake in mice

To investigate whether long term excessive intake of RIZ can induce a preference for RIZ in mice, we designed a self- selected drug administration protocol for freely

moving mice. The mice were allowed to choose between drinking water and RIZ solution. During this process, mice exposed to repeated NTG stimulation showed a more pronounced preference for RIZ. To avoid differences in drug consumption between the two bottles due to chance, we included an NS + DDW group that provided only two bottles of water. After excluding the influence of random selection on liquid consumption from the two bottles, we observed that the ratio of RIZ consumption to total liquid consumption in the NTG + RIZ group was consistently greater than 0.5 and exhibited a fluctuating upward trend as the experimental days increased. In contrast, the ratios of water consumption from the corresponding bottles in the other three groups fluctuated around 0.5 over time. The RIZ/RIZ + VEH ratio in the NTG + RIZ group was significantly greater than those in the other groups on Days 4 (NS + RIZ group vs. NTG + RIZ group: $p = 0.0002$, NS + DDW group vs. NTG + RIZ group: $p = 0.1655$), 6 (NS + RIZ group vs. NTG + RIZ group: $p = 0.0241$), 8(NS + RIZ group vs. NTG + RIZ group: $p = 0.0304$, NTG + DDW group vs. NTG + RIZ group: $p = 0.0327$), 10(NS + DDW group vs. NTG + RIZ group: $p = 0.0180$, NS + RIZ group vs. NTG + RIZ group: $p = 0.0014$, NTG + DDW group vs. NTG + RIZ group: $p = 0.0017$), 12(NS + RIZ group vs. NTG + RIZ group: $p = 0.0031$, NTG + DDW group vs. NTG + RIZ group: $p = 0.0024$), and 14(NS + RIZ group vs. NTG + RIZ group: $p = 0.0390$). Additionally, the RIZ or VEH/VEH ratio was significantly greater on Days 10(NTG + DDW group vs. NTG + RIZ group: $p = 0.0307$) and 12(NTG + DDW group vs. NTG + RIZ group: $p = 0.0272$) than in the other three groups and showed an increasing trend (Fig. 1D).

These results indicate that mice exposed to chronic NTG stimulation indeed exhibited a stable preference for RIZ, which increased in a fluctuating manner with the number of days of RIZ consumption. This pattern of change was not observed in the NS + RIZ group. There was no significant change in the body weights of the mice after RIZ administration (Supplementary Materials 5).

Repeated administration of RIZ in NTG mice induces a prolonged state of latent sensitization

To verify whether excessive use of RIZ induces potential pain sensitization in NTG model mice, we administered a low dose of a nitric oxide donor, SNP (0.03 mg/kg), on Days 40 of model establishment (when pain thresholds returned to baseline). Behavioural measurements were taken at 1, 2, 3, 4, and 5 h after SNP administration. Observations of the mechanical pain threshold data revealed that, after SNP stimulation, the NTG + RIZ group exhibited a rapid decrease in mechanical pain thresholds, specifically in the head and hind paw, with a slower recovery than in the other three groups ($p < 0.01$) (Fig. 1C).

Continuous administration of RIZ exacerbates NTG-induced anxious behaviour

Patients with MOH are significantly associated with emotional disorders such as anxiety and depression [37]. Studies have shown that patients with MOH with comorbid emotional disorders face more complex withdrawal treatments, which are characterized by poor therapeutic outcomes and a greater likelihood of relapse [38–40]. In our daily breeding of mice, we observed that in the drug administration phase, NTG-mediated model mice with excessive intake of RIZ were more prone to exhibit irritability, agitation, increased activity, and heightened vigilance. To investigate whether the overuse of RIZ induces emotional disorders such as anxiety and irritability in mice, we conducted the EPM and OFT. Forty mice were initially included (20 per group). However, one mouse did not complete the test because of health issues (overgrown incisors leading to insufficient food intake and subsequent body weight loss of over 20%), and another mouse did not complete the test because it escaped. Therefore, the final sample size per group was 18. Compared with those in NS + DDW group, in the EPM test, the NTG + RIZ group of mice had a significantly lower ratio of time in the open arms/total time (NTG + RIZ vs. NS + DDW = 0.1035 ± 0.01488 vs. 0.1897 ± 0.02549, $p = 0.0061$), a lower proportion of entries into the open arms (NTG + RIZ vs. NS + DDW = 0.1089 ± 0.01413 vs. 0.2021 ± 0.01845, $p = 0.0003$), a higher ratio of time in closed arms/total time (NTG + RIZ vs. NS + DDW = 0.6778 ± 0.02645 vs. 0.4711 ± 0.03608, $p < 0.0001$), and a higher proportion of entries into the closed arms (NTG + RIZ vs. NS + DDW = 0.3893 ± 0.0138 vs. 0.3178 ± 0.01331, $p = 0.0007$) (Fig. 1E). In the OFT, the NTG + RIZ group of mice had significantly shorter residence time in the central zone (NTG + RIZ vs. NS + DDW = 7.3483 ± 1.41654 vs. 33.6394 ± 3.33586, $p < 0.0001$), freezing time in the central zone (NTG + RIZ vs. NS + DDW = 0.4083 ± 0.3404 vs. 3.8133 ± 1.16892, $p = 0.0084$), activity distances in the central zone (NTG + RIZ vs. NS + DDW = 1698.7961 ± 192.52794 vs. 5958.3411 ± 481.60935, $p < 0.0001$), and number of entries into the central zone (NTG + RIZ vs. NS + DDW = 6.5000 ± 0.70131 vs. 20.6111 ± 1.74359, $p < 0.0001$) than did the NS + DDW group (Fig. 1F).

Exploration of specific brain regions in AI-MOHM mice

To detect the distribution of activated brain regions in the active ingestion-induced medication overuse headache model (AI-MOHM) and to validate AI-MOHM at the histological level, we assessed the activation levels in

different brain regions by performing c-Fos immunofluorescence staining on mice from the four groups. Through manual counting of c-Fos positive neurons across the entire brain, we found that mice in the NTG + RIZ group had significantly greater numbers of c-Fos + cells than did those in the NS + DDW group. We identified and statistically analysed the 25 brain regions most relevant to the pathophysiological processes in MOH, which were significantly activated in the AI-MOHM (Supplementary Material 1, Fig. 2 and Supplementary Material 4). These regions included the ventral orbital cortex (VO), lateral orbital cortex (LO), prelimbic cortex (PrL), cingulate cortex area 1 (CG1), cingulate cortex area 2 (CG2), nucleus accumbens shell and core (AcbSh, AcbC), lateral septal nucleus (LS), insular cortex (IC), paraventricular thalamic nucleus anterior part (PVA), central medial thalamic nucleus (CM), bed nucleus of the stria terminalis (BNST), peduncular part of the lateral hypothalamus (PLH), paraventricular hypothalamic nucleus (PT), anterior parvicellular (PaAP), anterior hypothalamic area (AH), dorsomedial hypothalamic nucleus (DM), ventral hippocampus cortex (vHPC), basolateral amygdaloid nucleus anterior part (BLA), central amygdaloid nucleus (CeA), lateral habenular nucleus (LHb), xiphoid thalamic nucleus (Xi), ventral tegmental area (VTA), periaqueductal grey (PAG), and spinal trigeminal nucleus caudal part (SPVC). We used MRIcroGL and Python 3.11 for data visualization of c-Fos counts and anatomical presentation based on the ALLEN Mouse Atlas (Fig. 2A).

To standardize the data, we used the c-Fos counts from the NS + DDW, NS + RIZ, and NTG + DDW groups as baselines and applied Z score normalization to the NTG + RIZ data. This approach successfully eliminated differences in signal amplitude among experimental groups that might otherwise obscure true biological characteristics, allowing for the comparison of experimental data on a common scale. The Z score represented the normalized c-Fos expression in the three paired groups, which was calculated based on the mean and standard deviation of their respective control groups. Statistical analysis involved comparing the Z scores with a null distribution with a mean of zero and adjusting for multiple comparisons via the Benjamini–Hochberg method at a 5% false discovery rate. Compared with the NS + DDW group, the NTG + RIZ group presented upregulated expression in all 25 brain regions (Fig. 2B), which was consistent with the direct statistical results of the immunofluorescence staining. Compared with the NS + RIZ group, the NTG + RIZ group presented upregulated expression in 13 brain regions, including the Xi, SPVC, PVA, PrL, PaAP, MO, LS, and IC ($p < 0.05$), whereas downregulation was observed in 3 brain regions, namely, the VTA, lateral periaqueductal grey (LPAG), and AH ($p < 0.05$) (Fig. 2C). Compared with the NTG + DDW group, the NTG + RIZ group presented significant upregulation of 20 brain regions, including the Xi, VTA, VO/LO, PVA, AcbSh, and AcbC ($p < 0.05$), with no clear downregulation in any other brain region (Fig. 2D). The Z scores of NS + RIZ vs. NTG + DDW, NS + RIZ vs. NS + DDW, NTG + DDW vs. NS + DDW can be found in Supplementary Material 1, Fig. 1.

After data normalization, hierarchical clustering was applied to the standardized data.

This method is particularly effective in brain region data analysis because it can simultaneously reveal functional associations and modular structures among brain

(See figure on next page.)

Fig. 1 Overuse of RIZ Enhances Potential Nociceptive Sensitization Induced by Repeated NTG Interventions **A.** Experimental flowchart for behavioural testing. RIZ: rizatriptan. NS: normal saline. NTG: nitroglycerin. i.p.: intraperitoneal injection. p.o.: peros. EPM: elevated plus maze. OFT: open field test. **B** Comparison of trends in hind paw mechanical pain thresholds over time during modelling and during withdrawal among the four groups (left). *$p < 0.05$, **$p < 0.01$, ***$p < 0.001$, ****$p < 0.0001$, NS + DDW group vs. NTG + RIZ group. $$p < 0.05$, $$$p < 0.01$, $$$$p < 0.001$, $$$$$p < 0.0001$ NS + DDW group vs. NTG + DDW group. &$p < 0.05$ NS + RIZ group vs. NTG + DDW group. ^$p < 0.05$, ^^$p < 0.01$, ^^^$p < 0.001$, ^^^^$p < 0.0001$ NS + DDW group vs. NS + RIZ group. @ $p < 0.05$, @@$p < 0.01$ NS + RIZ group vs. NTG + RIZ group. Comparison of trends in head mechanical pain thresholds over time during modelling and during withdrawal among the four groups (right). * $p < 0.05$, **$p < 0.01$ NS + DDW group vs. NTG + RIZ group. $$p < 0.05$, $$p < 0.01$ NS + DDW group vs. NTG + DDW group. &$p < 0.05$ NS + RIZ group vs. NTG + DDW group. ^$p < 0.05$, ^^$p < 0.01$ NS + DDW group vs. NS + RIZ group. The data are presented as the means ± SEMs. $n = 6$ mice per group. **C** Changes in mechanical nociceptive thresholds in the head and hind paw regions over 5 h following SNP stimulation in the four groups of mice. *$p < 0.05$, **$p < 0.01$, ***$p < 0.001$, ****$p < 0.0001$ (NS + DDW vs. NTG + RIZ). @$p < 0.05$, @@$p < 0.01$ (NS + RIZ vs. NTG + RIZ). #$p < 0.05$, ##$p < 0.01$, ###$p < 0.001$ (NTG + DDW vs. NTG + RIZ). ^$p < 0.05$ (NS + DDW vs. NS + RIZ). The data are presented as the means ± SEMs. $n = 6$ mice per group. **D** Temporal progression of active feeding behavioural patterns in the four experimental cohorts during the model establishment phase. $n = 6$ mice per group. **E** Comparative behavioural analysis in the EPM test and movement trajectory heatmaps between the NTG + RIZ and NS + DDW groups post-modelling. The heatmap spectrum reflects the dwelling time distribution across spatial coordinates, ranging from deep blue (minimal duration) to bright yellow (maximal duration). Structural delineations: Thinner borders denote open arms, and thicker borders represent closed arms. The number of experimental animals per group was 18. **F** Open field behavioural comparison between the NTG + RIZ and NS + DDW groups post-modelling. The thermal gradient illustrates the spatial dwelling time from deep blue (lowest) to bright yellow (highest). The inner quadrant demarcates the central zone, with the annular region between the inner and outer quadrants defining the peripheral area. **$p < 0.01$, ***$p < 0.001$, ****$p < 0.0001$, NS + DDW group vs. NTG + RIZ group. $n = 18$ mice per group

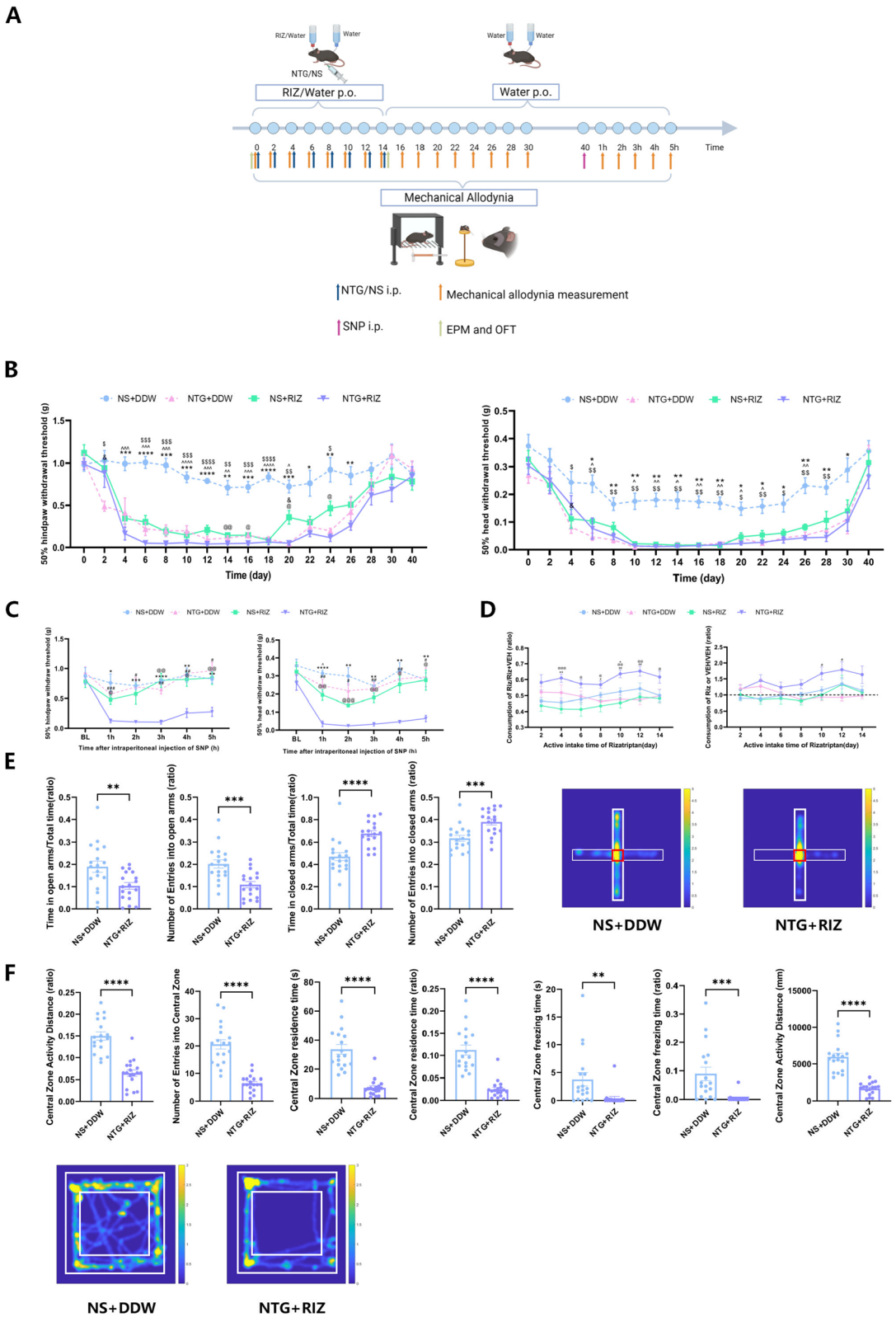

Fig. 1 (See legend on previous page.)

regions. The specific number of clusters was determined by combining the number of evaluation criteria and the anatomical connections of the brain regions (comprehensive classification schemata are delineated in the Results). The hierarchical clustering results were presented in the form of dendrograms, which intuitively displayed functional patterns among brain regions by grouping those with higher similarity into the same cluster. Following the clustering analysis, we further adjusted the clusters based on the brain region connections shown in existing studies. The NTG + RIZ vs. NS + DDW group was clustered into 4 clusters (Fig. 2E), with the cluster formed by CM, SPVC, DM, VO/LO, and LS showing the most significant differences in upregulation. The NTG + RIZ vs. NS + RIZ group was clustered into 4 clusters (Fig. 2F), with CM forming a separate cluster that presented the most significant upregulation differences, whereas the clusters formed by AH, VLPAG, vHPC, VTA, and LPAG presented the most significant downregulation differences. The NTG + RIZ vs. NTG + DDW group was clustered into 4 clusters (Fig. 2G), with the cluster formed by CM and DM showing the most significant differences in upregulation. The hierarchical clustering results of the NS + RIZ vs. NTG + DDW, NS + RIZ vs. NS + DDW, and NTG + DDW vs. NS + DDW groups are provided Supplementary Material 1, Fig. 1.

Network analysis and hub Identification

Based on the calculation of brain region correlation matrices, this study further explored the functional connections between brain regions. The Pearson correlation coefficient was used as a metric to quantify the strength of functional associations between brain regions, with results presented in the form of heatmaps to rapidly identify significant interregional correlations. The calculation of correlation matrices allows for the quantification of functional synchrony between different brain regions, providing foundational data for subsequent network modelling.

Hubs are nodes that occupy critical central positions within a network and are essential for its normal functioning. This analysis assessed node importance using degree (number of direct connections), betweenness centrality (proportion of shortest network paths passing through a node), and eigenvector centrality (influence based on the centrality of connected nodes). The values of degree centrality, betweenness centrality, and eigenvector centrality calculated via the BCT analysis package were used to screen brain regions with all variable values in the top 10%, which were identified as hub regions. SPVC and PrL, characterized by their high degree and eigenvector centralities, as well as their significantly higher betweenness centrality, underscore their key roles in propagating and integrating neural signals within the AI-MOHM mouse network. By integrating the hierarchical clustering analysis results, we found that the neural network connections between the PrL/IC and SPVC brain regions may play a core role in the development of the AI-MOHM mouse model (Fig. 2E and J). The results of network analysis combined with clustering analysis suggest that, compared with NS + RIZ group, the connections between the PrL/IC/VO/LO and SPVC/BLA/AcbSh/PLH neural networks may play a significant role (Fig. 2F and H). Compared with those of NTG + DDW group, the PrL/IC and SPVC/AcbSh networks may be crucial (Fig. 2G and I).

After withdrawing RIZ and NTG, the pain thresholds in the withdrawal group gradually improved, but anxiety-like behaviour did not significantly change

This experiment simulated withdrawal-based analgesic drug treatment in patients with MOH and compared the behavioural and histological changes between AI-MOHM model mice and those after withdrawal termination. A total of 14 mice were used for modelling, and behavioural assessments were conducted on Days 14 after model establishment. Two mice died due to a technical error during intraperitoneal injection;

(See figure on next page.)

Fig. 2 Exploration of Specific Brain Regions in AI-MOHM Mice. **A** An illustration of the expression levels of c-Fos in 25 brain regions of the four groups of mice after the model was established is presented. $n = 3$ or 4 mice per group. **B-D** Compared with the other three groups of mice (NS + DDW group, NTG + DDW group, NS + RIZ group), the NTG + RIZ group exhibited different expression of c-Fos in 25 different brain regions (*$p < 0.05$, **$p < 0.01$, ***$p < 0.001$). **E–G** Hierarchical clustering analysis was performed on the three paired groups based on the Z-values, and brain regions with greater similarity were clustered together. The heatmap displays the correlation of log c-Fos density in 25 brain regions (selected through a literature review) across different paired groups. The correlation was colour-coded based on the Pearson coefficient. The network analysis diagram revealed significant positive correlations between regions ($p < 0.05$), with Pearson's r exceeding 0.82. The thickness of the edges represented the degree of association, and the size of the nodes represents the number of connections (degree). The colour of the nodes indicates the betweenness centrality, with the spectrum ranging from dark blue (highest) to dark red (lowest). Hubs are marked in bright yellow in the diagram. **H-J** Brain network connectivity maps of three paired groups. Except for the bright yellow colour of the hubs, the colours of the other brain regions were consistent with the colour spectrum of the correlation heatmap. For the above related data, please refer to Supplementary Material 3

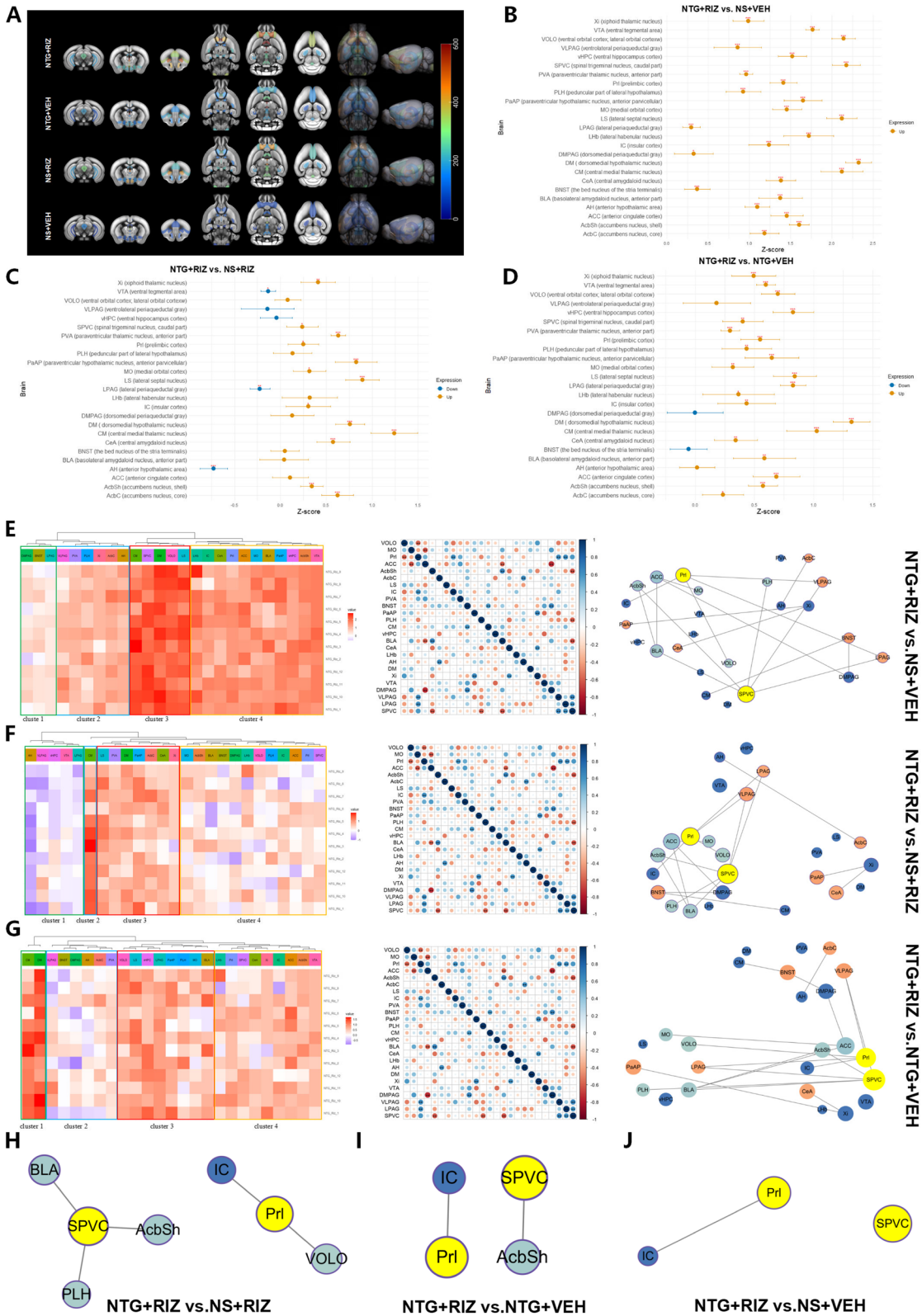

Fig. 2 (See legend on previous page.)

therefore, the final sample size was 12 mice. Six mice were randomly selected as the control group (Model group) using the random number table method, and brain tissues from these mice were harvested for immunofluorescence staining. The remaining mice in the withdrawal treatment group (Withdraw group) were withdrawn from RIZ and NTG, and behavioural and histological evaluations were performed after the withdrawal intervention (Fig. 3A). Sixteen days after withdrawal, the hind paw pain threshold (Model vs. Withdraw = 0.009 ± 0.00045 vs. 0.1033 ± 0.01606, $p <$ 0.001) and head pain threshold (Model vs. Withdraw = 0.01 ± 0 0.00 vs. 0.05 ± 0.006325, ****$p <$ 0.0001) in the Withdraw group increased significantly (Fig. 3B). Compared with the Model group, the Withdraw group did not have statistically significant differences in residence time in the central zone of the open field (Model vs. Withdraw = 10.97 ± 3.353948 vs. 10.9967 ± 2.510942, $p =$ 0.9950), freezing time in the central zone of the open field (Model vs. Withdraw = 0.8238 ± 0.596663 vs. 1.3977 ± 0.650682, $p =$ 0.5119), number of entries into the central zone (Model vs. Withdraw = 8 ± 0.774597 vs. 8 ± 1.549193, $p >$ 0.9999) (Fig. 3C), the ratio of the time in the open arms/total time (Model vs. Withdraw = 0.121946176 ± 0.031418 vs. 0.069853801 ± 0.026196, $p =$ 0.2317), the proportion of entries into the open arms (Model vs. Withdraw = 0.129885456 ± 0.023392 vs. 0.101791348 ± 0.029914, $p =$ 0.4764), the ratio of the time in the closed arms/total time ratio (Model vs. Withdraw = 0.674283142 ± 0.061168 vs. 0.663193916 ± 0.043220, $p =$ 0.8852), or the proportion of number of entries into the closed arms (Model vs. Withdraw = 0.370114544 ± 0.0233919369 vs. 0.401938516 ± 0.032677, $p =$ 0.4468)between the two groups of mice (Fig. 3D).

During the modelling period, the pain threshold of the mice subjected to the gepant intervention slowly decreased, but the intervention had no effect on negative emotions

From D0 to D14 of AI-MOHM modelling, rimegepant (Gepant) was administered via intraperitoneal injection every other day to explore its role in the model formation process (Fig. 4A). Mechanical pain thresholds of the head and hind paw were measured in the experimental group (RIZ + NTG + Gepant) and the control group (RIZ + NTG + VEH) (two-way repeated-measures ANOVA with Tukey post hoc test (left): main group effect: F (1, 25) = 18.95, $p =$ 0.0002; main time effect: F (2.334, 58.36) = 24.26, $p <$ 0.0001; group × time interaction: F (7, 175) = 3.357, $p =$ 0.0022;two-way repeated-measures ANOVA with Tukey post hoc test (right): main group effect: F (1, 21) = 27.81, $p <$ 0.0001; main time effect: F (2.750, 85.26) = 105.0, $p <$ 0.0001; group × time interaction: F (7, 217) = 2.450, $p =$ 0.0195). Thirty mice were initially involved. Among them, 3 mice in the same cage were excluded because of possible ulcerative dermatitis, resulting in a sample size of 12 for the RIZ + NTG + Gepant group. The sample size in the RIZ + NTG + VEH group was 15. Compared with the RIZ + NTG + VEH group, the RIZ + NTG + Gepant group presented significantly greater mechanical pain thresholds in the head on Days 6, 8, and 10 and in the hind paw on Days 4, 6, 8, 10, and 12 ($p <$ 0.05) (Fig. 4B). On Days 14, model was established, the EPM and OFT were conducted on both groups of mice. The results indicated that during the modelling period, Gepant intervention did not significantly affect the ratio of time in the open arms/total time (RIZ + NTG + VEH vs. RIZ + NTG + Gepant = 0.100542495 ± 0.0208370882 vs. 0.064801283 ± 0.0124280275, $p =$ 0.1580), the proportion of entries into the open arms (RIZ + NTG + VEH vs. RIZ + NTG + Gepant = 0.168965361 ± 0.0238744237 vs. 0.197498598 ± 0.0367155775, $p =$ 0.5229), the ratio of time spent in

(See figure on next page.)

Fig. 3 Withdraw Intervention Restored Cutaneous Mechanical Allodynia. **A** Experimental flowchart for behavioural testing and grouping. **B** Changes in the mechanical pain thresholds of the head and hind paw in AI-MOHM mice after 16 days of withdrawal intervention. ***$p <$ 0.001, ****$p <$ 0.0001, $n =$ 6 per group. **C** Changes in open field behaviour and heatmap of the trajectories in AI-MOHM mice after 16 days of withdrawal intervention. The spectrum of the heat map represents how long the mice stayed at different points, ranging from dark blue (lowest) to bright yellow (highest). The inner square represents the central area, and the area composed of the outer and inner squares represents the peripheral part. $n =$ 6 per group. **D** Changes in EPM behaviour and the heatmap of the trajectories of AI-MOHM mice after 16 days of withdrawal intervention. The spectrum of the heatmap represents how long the mice stayed at different points, ranging from dark blue (lowest) to bright yellow (highest). The thinner border represents the open arm, and the thicker border represents the closed arm. $n =$ 6 per group. **E.** Double immunofluorescence images showing the changes in c-Fos expression in the PrL, IC, and SPVC brain regions after the withdrawal of intervention in the mice. Red fluorescence represents c-Fos, green fluorescence represents NeuN, and white triangle arrows are used to indicate co-stained neurons. The specific distribution of the brain regions is indicated by white dashed lines in the fluorescence scanning image, scale bar: 40 μm. $n =$ 3 or 4 mice per group. **F.** Quantitative analysis of the relative density distribution of c-Fos in the three brain regions ($n =$ 12 sections); ****$p <$ 0.0001 for the Model group vs. the Withdraw group

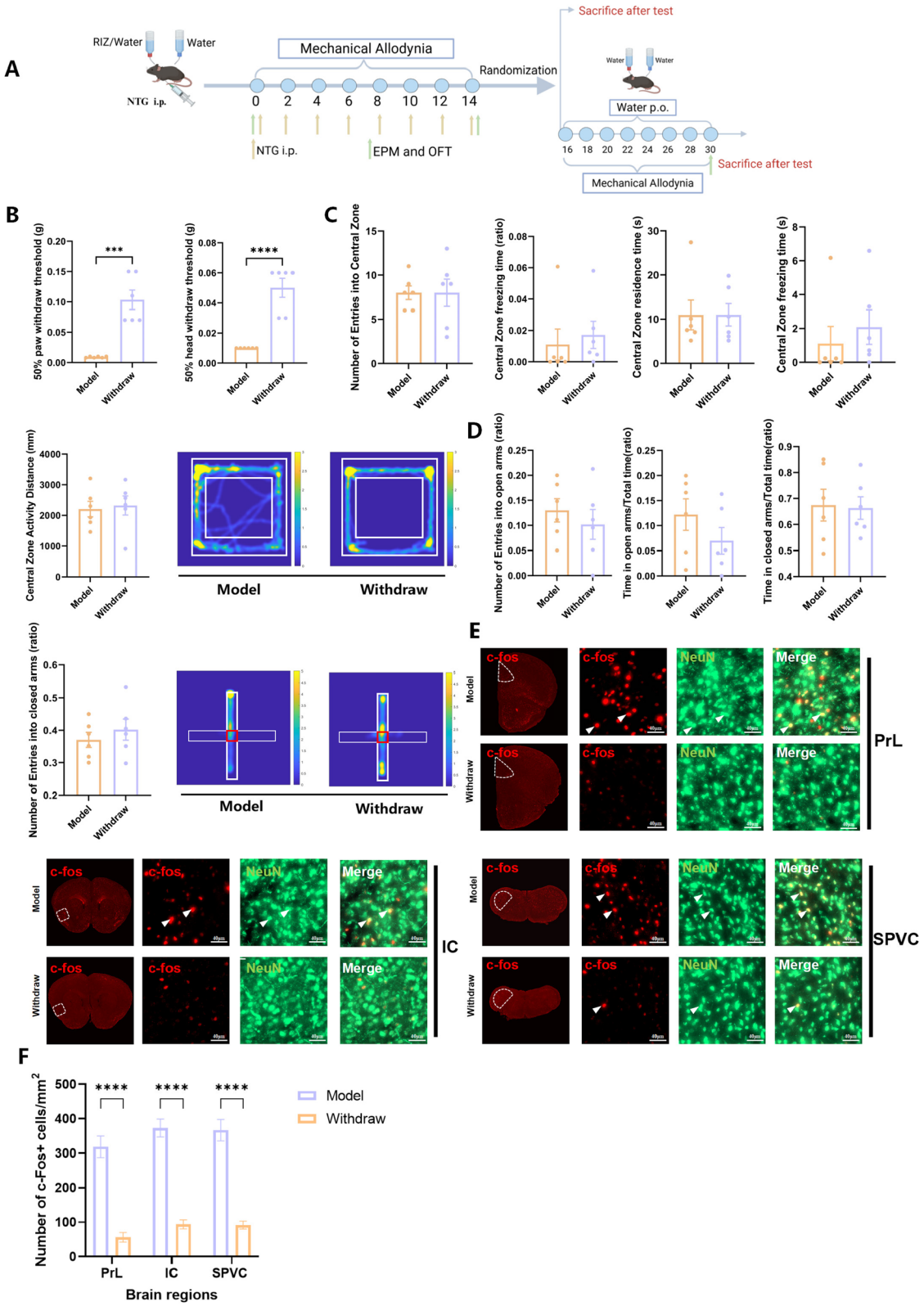

Fig. 3 (See legend on previous page.)

the closed arms/total time (RIZ + NTG + VEH vs. RIZ + NTG + Gepant = 0.716303941 ± 0.0333307293 vs. 0.798926335 ± 0.0281816947, $p = 0.0746$), or the proportion of entries into the closed arms (RIZ + NTG + VEH vs. RIZ + NTG + Gepant = 0.581034639 ± 0.071809 vs. 0.604449454 ± 0.070268406, $p = 0.8184$) (Fig. 4C and D). In the OFT, residence time in the central zone of the open field (RIZ + NTG + VEH vs. RIZ + NTG + Gepant = 19.804 ± 9.337654 vs. 18.365 ± 7.207690, $p = 0.6687$), activity distance in the central zone (RIZ + NTG + VEH vs. RIZ + NTG + Gepant = 2611.002 ± 1004.759806 vs. 1206.97 ± 232.402122, $p = 0.1382$), and number of entries into the central zone (RIZ + NTG + VEH vs. RIZ + NTG + Gepant = 8.4 ± 2.694439 vs. 5 ± 1.183216, $p = 0.1531$) were not significantly different between the two groups of mice (Fig. 4E and F). Ten mice per group were subjected to the EPM test and OFT, and all mice completed the EPM test. Four mice were excluded because the baseline criteria were not met; thus, six mice per group were used for the OFT at baseline. Unfortunately, one mouse in the RIZ + NTG + VEH group died of error operation during NTG injection before the OFT. The final sample sizes of the mice that completed the OFT were as follows: RIZ + NTG + VEH group, 5 mice; RIZ + NTG + Gepant group, 6 mice.

Withdrawal treatment after the modelling phase and rimegepant intervention during the modelling phase resulted in decreases in c-Fos activation in the PrL, SPVC, and IC brain regions

After pain behaviour and emotional assessments were completed, c-Fos immunofluorescence staining was performed on the brains of the mice in the different groups, and the number of c-Fos-positive cells was quantified. Compared with those in the AI-MOHM group, c-Fos activation in the PrL, SPVC, and IC regions significantly decreased following withdrawal (PrL: Model vs. Withdraw = 318.75 ± 30.945486 vs.56.25 ± 13.804986; IC: Model vs. Withdraw = 372.92 ± 26.013242vs.93.75 ± 13.101078; SPVC: Model vs. Withdraw = 366.67 ± 30.977346 vs. 91.67 ± 11.650422) (****$p <$ 0.0001) (Fig. 3E and F). Similar results were observed after rimegepant intervention (PrL: RIZ + NTG + Gepant vs. RIZ + NTG + VEH = 219.05 ± 19.738224 vs.534.52 ± 23.047324; IC: RIZ + NTG + Gepant vs. RIZ + NTG + VEH = 136.9 ± 14.394428 vs. 516.67 ± 25.954019; SPVC: RIZ + NTG + Gepant vs. RIZ + NTG + VEH = 96.43 ± 12.827346 vs. 576.19 ± 32.250701) (****$p <$ 0.0001) (Fig. 4G and H).

Discussion

Currently, both clinical and basic research studies agree that the onset of MOH is closely related to central sensitization in the nervous system [52, 53]. In the process of MOH development, both excessive use of acute analgesics and pre-existing primary headache disorders are indispensable factors. Moreover, the roles of biological behavioural factors in the progression of MOH should not be overlooked [54]. Therefore, the interaction between headaches and drug abuse is highly complex, and there is an urgent need for a more accurate preclinical model that reflects the clinical characteristics of patients with MOH to support further mechanistic research. Various animal models for MOH have been developed in past studies [35, 53, 55], but they all share the common feature of passive administration of analgesics to mice. Furthermore, some models lack effective pain stimulation [56, 57]. In this study, we induced migraine-like headaches in mice using repeated intraperitoneal injections of NTG and gradually established chronic migraine-like pain through intermittent injection. During this process, we provided a specific concentration of RIZ solution and water for the mice to self-administer. This self-administration procedure is similar to the fentanyl self-administration paradigm studied by Terem A and colleagues [58]. AI-MOHM mice were subjected to short-term stimulation

(See figure on next page.)

Fig. 4 Rimegepant Intervention during the Modelling Period Slowed the Decline in the Pain Threshold. **A** Experimental flowchart for behavioural testing. **B** Temporal progression of mechanical allodynia thresholds in the head and hind paw of AI-MOHM mice following rimegepant intervention during modelling. *$p < 0.05$, **$p < 0.01$, ***$p < 0.001$, ****$p < 0.0001$ RIZ + NTG + Gepant vs. RIZ + NTG + VEH. $n = 12$ in the RIZ + NTG + Gepant group and $n = 15$ in the RIZ + NTG + VEH group. **C-D** Comparative behavioural profiling in the EPM (**C**) and movement trajectory heatmaps (**D**) between prophylactically rimegepant-treated and control cohorts at the modelling endpoint. Heatmap gradients reflect spatial dwelling durations (spectral range: deep blue [minimum] to bright yellow [maximum]). Structural annotations: thin borders, open arms. thick borders, closed arms. $n = 10$ per group. **E–F** Open field behavioural analysis (**E**) and locomotion heatmaps (**F**) after prophylactic rimegepant administration. Thermal encoding indicates the residence time distribution (spectral range: deep blue to bright yellow). Spatial demarcations: inner quadrant, central zone; outer area between inner/outer quadrants, peripheral annular region. RIZ + NTG + Gepant group: $n = 6$; RIZ + NTG + VEH group: $n = 5$. **G** Dual immunofluorescence visualization of c-Fos/NeuN colocalization in the PrL (prelimbic cortex), IC (insular cortex), and SPVC (spinal trigeminal nucleus caudal subnucleus) following rimegepant intervention. Red: c-Fos; green: NeuN; white arrowheads: co-labelled neurons. The dashed white contours indicate anatomical boundaries; scale bar: 40 μm. **H.** Quantitative analysis of c-Fos + neuronal density in specified brain regions. $n = 3$ or 4 mice per group. ****$p < 0.0001$ RIZ + NTG + Gepant group vs. RIZ + NTG + VEH group

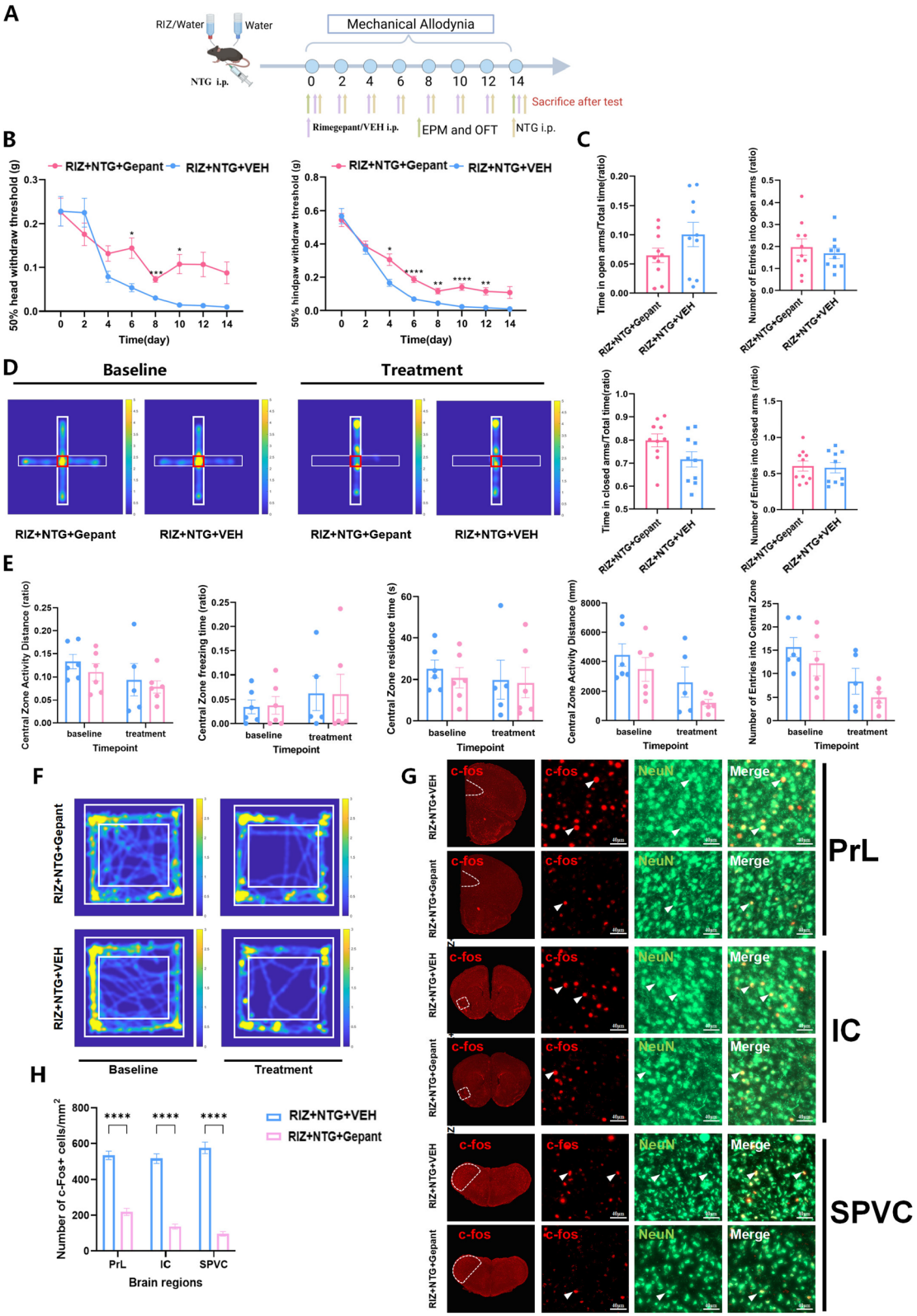

Fig. 4 (See legend on previous page.)

without invasive procedures such as gavage [55], which causes significant trauma, or subcutaneous implantation of micro-osmotic pumps [35], which involves continuous foreign body insertion. By analysing the consumption of the RIZ solution, we assessed preference of the mice for triptans, thereby simulating the medication overuse observed in patients with MOH. This method of allowing mice to self-administer acute pain medications not only serves as an experimental approach but also introduces a new way to assess drug preference, which has not been explored before. We defined the mouse model established using this approach as the active ingestion-induced medication overuse headache model. We subsequently validated AI-MOHM through both behavioural and histological assessments. AI-MOHM exhibits behavioural characteristics similar to those of traditional models and patients with medication overuse: 1) sensitization, 2) activation, 3) active ingestion, and 4) anxiety and depression. Histologically, the activated brain regions in AI-MOHM are highly similar to those observed in previous headache models and in functional imaging studies of patients with medication overuse headache [54]. These results indicate that AI-MOHM is a reliable model.

The involvement of addiction in the occurrence and development of MOH has always been controversial [10, 59]. In terms of behaviour, sensitization is a common feature of addiction and MOH, although the expressions are different. In chronic headache, sensitization mainly manifests as allodynia, which is a painful sensation caused by harmless stimuli (such as light touch). Cutaneous allodynia is a sign of central sensitization, which involves the action of pronociceptive mediators and increases the response of nociceptors [60]. In drug addiction, sensitization occurs after repeated (usually intermittent) administration of drugs of abuse, manifested as increased locomotor activity in mice [61], or increased activity/energy levels, mood, speech volume, and blink rate in humans [62]. The increased drug effect after repeated administration reflects sensitization of the corticolimbic system in the brain [63–65]. Moreover, sensitization of the brain reward system can further motivate the desire for drugs and drug cues, which may lead to pathological "cravings" for drugs [66, 67]. In patients with MOH, certain behaviours may also occur, such as ritualized drug administration [68, 69], psychological drug attachment, and withdrawal symptoms, which are considered to be related to drug addiction [70]. According to the incentive sensitization theory, dopamine can regulate the desire to take drugs, which is distinct from liking drugs [67]. In other words, owing to the lack of beneficial effects produced by drug tolerance, drug users can continue to desire drugs, even if they no longer like them. According to this theory, patients with MOH may also desire to take analgesics, despite the lack of analgesic effects. Therefore, people hope to continue taking analgesics, which can be transformed into a psychological attachment. This attachment may prompt patients with MOH to take analgesics routinely every morning, despite the lack of benefits or positive outcomes. Further research is needed to clarify whether these behaviours develop into compulsive behaviours. In our study, the active intake of RIZ in AI-MOHM mice continued to increase with increasing modelling time and the mice were clearly preferable to drinking RIZ. This state persisted even after chronic NTG stimulation was withdrawn. In the early stages of withdrawal, AI-MOHM mice also exhibited severe emotional disorders, which manifested as irritability, anxiety, mania, aggressive behaviour, and increased activity, similar to the withdrawal symptoms of drug addiction. In the first phase of the experiment, we performed c-Fos immunofluorescence staining on the four groups of mice to screen specific brain regions. Hierarchical clustering analysis and network analysis indicated that the SPVC and PrL regions in the AI-MOHM mouse network were defined as hub brain regions.

Research on MOH has largely focused on cases where the primary headache is chronic migraine, and the mechanisms of MOH without chronic migraine have not been thoroughly investigated. However, previous studies have shown no significant difference in depression and anxiety levels between MOH derived from chronic tension-type headache and those derived from chronic migraine [71]. Notably, individuals with no history of primary headache who use acute analgesics for other pain conditions have not reported developing medication overuse headache [72]. Our study revealed that mice treated with only analgesics also experienced a decrease in the pain threshold, which is consistent with previous studies in which analgesics were passively administered to establish MOH models [13, 18, 35, 55]. In this study, the pain threshold decline in NS + RIZ group mice after SNP application was not significant, suggesting that NTG-induced analgesic overuse led to more persistent and severe central sensitization. This result also suggests that MOH caused by chronic migraine results in more severe central sensitization than MOH caused by other types of primary headaches [73].

Hierarchical clustering and network analysis revealed that, compared with the NS + RIZ group, the SPVC region plays a central role in the network. The SPVC is a key area for processing head and facial pain signals, especially in patients with migraine, as it receives noxious input from the trigeminal nerve and transmits this information to the thalamus and higher brain regions [31]. Studies have shown that SPVC activity is significantly elevated in patients with migraine and is correlated with

pain intensity [74, 75]. Animal studies also indicate that long-term use of analgesics can lead to neuroplastic changes in SPVC, increasing pain sensitivity [55]. Furthermore, functional impairment of the SPVC can lead to increased pain-related anxiety and depressive behaviours [37]. In our study, as the modelling time progressed, the amount of RIZ consumed by the AI-MOHM mice continued to increase, and they exhibited a clear preference. This state persisted even after chronic NTG stimulation ceased. Early withdrawal revealed that the AI-MOHM mice still exhibited significant emotional disturbances, including irritability, anxiety, mania, aggressive behaviour, and increased activity, resembling the withdrawal symptoms of drug addiction.

The PrL is part of the medial prefrontal cortex and has fibre connections with the orbital cortex [76], accumbens nucleus [77], amygdala [78], insular cortex [79], and other cortical and subcortical areas. It is extensively involved in the regulation of pain and related anxiety-depressive behaviours [80–82], fear [83], attention control [84], cognition [85], learning and memory [86], and social activities [87]. Changes in the reward system are a characteristic of MOH. MRI studies in patients with MOH have shown reduced resting-state functional connectivity between the ventral striatum (vSTR) and ventromedial prefrontal cortex (VMPFC), and the strength of connectivity between the VMPFC and bilateral vSTR was inversely correlated with the monthly intake of acute analgetic [88]. To date, no preclinical studies have reported the specific mechanistic role of PrL-involved addiction-related neural circuits in MOH, and more work is needed to further elucidate this mechanism. However, circuit studies on addictive substances may provide insights for future research. Goal-oriented action is a crucial component of our behavioural repertoire, enabling us to "control our environment to serve our desires and needs" [89]. Inhibiting the cytoskeletal regulatory factor Rho kinase in PrL promotes goal-directed decision-making and blocks habitual responses to cocaine [90]. Dysfunction in the PrL has been linked to drug dependence. Long-term cocaine self-administration reduces the ex vivo intrinsic excitability of deep-layer pyramidal neurons in the prelimbic cortex, promoting the development of compulsive drug-seeking behaviour [91]. The use of addictive substances affects various brain regions involved in reward regulation, such as the amygdala and nucleus accumbens, thereby triggering feelings of reward and initiating the development of addictive behaviour [92]. Subsequently, individuals often consciously associate the powerful rewarding properties of addictive substances with the environmental contexts in which these drugs are encountered, further promoting the formation of drug-related contextual memories [93]. Chen and colleagues [78] reported that the critical function of AdipoR1 in the $BLA^{CaMKII\alpha} \rightarrow PrL^{CaMKII\alpha}$ circuit in regulating methamphetamine-related memory formation. The activation of GABAB receptors in the granular insular cortex can disrupt the reconsolidation of morphine reward memory, eliminating established conditioned place preference to weaken the associative memory between drugs and drug-related contextual cues, thereby reducing the risk of relapse [94]. Additionally, projections from the granular insular cortex/lateral orbital cortex to the PrL promote the generation of compulsive behaviours [79]. Thus, the PrL may be involved in various aspects of addictive behaviours. In our study, the bottles containing the RIZ solution were marked and fixed in place for the mice to identify, simulating a fixed environment associated with acute analgesics. This can be regarded as a behavioural target the mice after NTG stimulation. With repeated NTG stimulation, the NTG + RIZ group of mice presented increased intake of RIZ. Hierarchical clustering analysis and network analysis revealed that the connection between the PrL and IC plays a critical role in the neural network. We speculate that PrL dysfunction, in addition to affecting pain- and emotion-related pathways, influences the cognitive and attention control systems of AI-MOHM mice, enhancing drug-seeking behaviour. The strengthening of the connection between the PrL and IC reinforced the relationship between acute analgesics and the environment, consolidating drug reward-related memories and promoting the development of MOH. This evidence supports the occurrence of addiction-like medication overuse behaviours during the development of MOH and explains the differences in brain activation and phenotypes between AI-MOHM mice and chronic migraine-like mice.

To further validate the roles of brain regions in the development of MOH, we conducted additional experiments for reverse verification. Limiting or withdrawing drugs is a key step in MOH treatment [54]. After AI-MOHM modelling was completed, withdrawal of the RIZ solution led to significant recovery of the mechanical pain thresholds in the head and hind paw, but there was no significant improvement in anxiety-like behaviours. Immunofluorescence staining revealed a marked reduction in c-Fos activation in the hub brain regions identified via the network analysis.

Over the past three decades, CGRP has been identified as a key factor in the pathogenesis of migraine [95, 96]. Various novel drugs targeting this pathway have emerged, among which CGRP receptor antagonists are the most representative. As a small molecule CGRP receptor antagonist that can cross the blood–brain barrier, rimegepant has shown good effects in the

management of migraine [97]; however, its role in the management of MOH remains unclear. Notably, clinical trials on rimegepant have indicated that frequent use does not induce MOH [98–100], suggesting that the CGRP system may play an unexpected role in the pathophysiology of MOH. Our study applied rimegepant intervention during the AI-MOHM modelling process, which slowed the decline in pain thresholds, but no significant improvement in anxiety-like behaviours was observed. This contrasts with our previous understanding of psychiatric comorbidities with MOH. Triptans can alleviate migraine by inhibiting the activation of nociceptors and blocking the peripheral release of vasoactive peptides, including substance P and CGRP [101]. However, long-term use of triptans may induce potential sensitization, increasing plasma CGRP concentrations under stress or nitric oxide (NO) donor induction [17]. Emerging research has gradually elucidated the relationship between triptans and the CGRP pathway. Chronic sumatriptan administration enhances NO synthase activity in trigeminal ganglion dural afferents, promoting NO-dependent hyperalgesia linked to CGRP release [13]. De Felice and colleagues [13] further elaborated on the specific mechanisms: sumatriptan exposure induced time-dependent allodynia, accompanied by a significant and persistent increase in CGRP-positive trigeminal fibre profiles and elevated blood CGRP levels in rodents. The CGRP receptor antagonist α-CGRP8-37 reversed this allodynia. Hagen and colleagues [35] explored the NO-CGRP release axis and demonstrated that chronic sumatriptan reduces PKA-Cα expression in trigeminal ganglia, promoting coupling between NO and Nav1.9 channels in dural afferent neurons via the NO-cGMP pathway. This lowers the susceptibility threshold for headache initiation factors, whereas Nav1.9 knockout prevents NO-induced CGRP release and mitigates central sensitization. CGRP monoclonal antibodies [17] prevent MOH formation by blocking CGRP-mediated signalling. Thus, drugs targeting CGRP pathways may act more directly on CGRP-related pathways to alleviate hyperalgesia in AIMOHM mice. Immunofluorescence staining results also revealed a significant reduction in the activation of hub brain regions. The number of CGRP-positive cells within the trigeminal ganglion also significantly decreased after rimegepant administration ($p = 0.0212$) (Supplementary Material 1 Fig. 3). However, whether rimegepant directly affects the CNS and leads to changes in its activation remains to be further confirmed. CGRP receptor antagonists have been proven to have antimigraine efficacy [102], but the specific sites of action remain unclear. CGRP and its receptor are widely expressed in multiple brain regions of the CNS, such as the cerebellum, thalamus, cerebral cortex, locus coeruleus, and SPVC [103, 104]. The blockade of CGRP receptors by the nonpeptide CGRP receptor inhibitor MK-8825 can prevent the increase in the activity of neurons in the SPVC after repeated NTG intervention, suggesting that CGRP may play an important role in the early stage of NTG-induced central trigeminal nerve activity [105]. A study using a positron emission tomography tracer (MK—4232) revealed that the application of a conventional dose of telcagepant (140 mg, p.o.) did not cause changes in brain activity, but when the dose was increased tenfold, it led to changes in brain activity [106]. In our study, after the application of a relatively high dose of rimegepant, the expression of c-Fos in the mouse brain changed. However, our experimental data cannot identify the site of action of rimegepant. Nevertheless, these behavioural and histological findings collectively suggest the potential of rimegepant in MOH management, providing a basis for clinical guidance in drug administration.

Conclusion

By combining pain stimulation and the active ingestion of analgesics, we developed a new mouse model that more accurately reflects the progression of MOH. The behavioural and histological characteristics of this model align well with the clinical features of patients with MOH. Immunofluorescence staining combined with hierarchical clustering analysis and network analysis expanded our understanding of the brain regions involved in the pathophysiology of MOH, highlighting the critical role of brain networks centred around the SPVC and PrL in MOH development. These findings provide potential targets for clinical neuro-modulatory therapies, especially for refractory MOH management. The preserved efficacy of rimegepant in this model suggests potential preventive applications for patients with high-risk MOH.

Limitations

MOH is more prevalent in females; thus, this study used female mice. However, further validation with male mice is necessary to confirm the conclusions drawn from this experiment. The results of this study strongly support the role of rimegepant in pain regulation, whereas the emotional behavioural outcomes did not significantly differ. This finding is inconsistent with the commonly observed comorbidity between headache and mood disorders. We speculate that CGRP receptor antagonists may primarily target pain regulatory pathways. However, it is also possible that the small sample size in certain behavioural assessments contributed to these results, and further studies with larger sample sizes are needed to explore

this issue. In addition, possibly because the mice were familiar with the testing arena, the EPM and OFT failed to yield statistically significant results. Regrettably, we were unable to present data on the precise regulation of selected brain regions and addiction-related neural circuits in this study, which represents the ongoing work of our team. To better demonstrate the effectiveness of the model protocol proposed in this study, we are continuing to explore the similarities and differences in brain region activation patterns under conditions of active versus passive analgesic intake.

Abbreviations

AcbC	Accumbens nucleus, core
AcbSh	Accumbens nucleus, shell
ACC	Anterior cingutate cortex
AH	Anterior hypothalamic area
AID	Agranular insular cortex
AI-MOHM	Active Ingestion-Induced Medication Overuse Headache Model
BLA	Basolateral amygdaloid nucleus, anterior part
BNST	Bed nucleus of the stria terminalis
CeA	Central amygdaloid nucleus
CeA	Central amygdaloid nucleus
CG1/2	Cingulate cortex area 1/2
CGRP	Calcitonin gene related peptide
CM	Central medial thalamic nucleus
CNS	Central nervous system
CSD	Cortical spreading depression
DAPI	4′, 6-Diamidino-2-phenylindole
DDW	Deuterium depleted water
DM	Dorsomedial hypothalamic nucleus
EPM	Elevated plus-maze
Gepant	Rimegepant
IC	Insular cortex
LHb	Lateral habenular nucleus
LO	Lateral orbital cortex
LPAG	Lateral periaqueductal gray
LS	Lateral septal nucleus
MOH	Medication overuse headache
MR	Magnetic resonance
MRI	Magnetic resonance imaging
NAc	Nucleus accumbens
NO	Nitric oxide
NTG	Nitroglycerin
OFT	Open field tests
PaAP	Paraventricular hypothalamic nucleus, anterior parvicellular
PAG	Periaqueductal gray
PBS	Phosphate buffer saline
PET	Positron emission tomography
PLA	People's Liberation Army
PLH	Peduncular part of lateral hypothalamus
PrL	Prelimbic cortex
PT	Paratenial thalamic nucleus
PVA	Paraventricular thalamic nucleus, anterior part
RIZ	Rizatriptan
RT	Room temperature
SNP	Sodium nitroprusside
SPF	Specific pathogen-free
SPVC	Spinal trigeminal nucleus, caudal part
VEH	Vehicle
vFF	Von Frey filament
vHPC	Ventral hippocampus cortex
VMPFC	Ventromedial prefrontal cortex
VO	Ventral orbital cortex
vSTR	Ventral striatum
VTA	Ventral tegmental area
Xi	Xiphoid thalamic nucleus

Supplementary Information

The online version contains supplementary material available at https://doi.org/10.1186/s10194-025-02066-4.

Supplementary Material 1.
Supplementary Material 2.
Supplementary Material 3.
Supplementary Material 4.
Supplementary Material 5.

Acknowledgements
Thanks to all members in our team for their valuable discussions and technical assistance. We acknowledge the developers of the following software: BioRender (https://biorender.com) used for Fig. 1 A, Fig. 3 A and Fig. 4 A. the Allen Software Development Kit v2.16.2 (https://allensdk.readthedocs.io/en/latest/) and MRIcroGL (https://github.com/neurolabusc/MRIcroGL10_OLD/blob) used for Fig. 2 A, Brain Connectivity Toolbox (https://sites.google.com/site/bctnet/, version 2019-03- 03) in MATLAB R2016a (The MathWorks Inc), Cytoscape (version 3.2.1), and MATLAB R2016a (Mathworks Inc) used for Fig. 2E-J.

Authors' contributions
SYY designed and supervised the study. RZL and ZD contributed to the study conceptualization and guidance. ZJM and CHL contributed equally to this work. WX, MJZ, HX, CCC, YL, WWZ, DQZ, and YYL performed experiments and acquired data. WJT and DFZ helped optimize the experimental process. ZJM, CHL, and WHB analyses data. ZJM and CHL wrote the paper. All authors read and approved the final manuscript.

Funding
This work was supported by the National Natural Science Foundation of China (grants 81471147, 81901145, 82271242).

Data availability
Data is contained within the article and supplementary materials. All data, reagents, resources, and protocols are available from the corresponding author upon reasonable requests.

Declarations

Ethics approval and consent to participate
The experimental procedures were approved by the Institutional Animal Care and Use Committee, Chinese PLA General Hospital, following the Regulations for the Administration of Affairs Concerning Experimental Animal.

Consent for publication
Not applicable.

Competing interests
The authors declare no competing interests.

Author details
[1]Department of Neurology, the, First Medical Centre, Chinese PLA General Hospital, Beijing 100853, China. [2]International Headache Centre, Chinese PLA General Hospital, Beijing 100853, China. [3]The 96607 Military Hospital of Chinese PLA, BaojiShaanxi Province 721000, China. [4]Shandong Institute of Brain Science and Brain-inspired Research, Shandong First Medical University & Shandong Academy of Medical Sciences, Jinan, Shandong Province 271016, China. [5]Department of Neurology, Aerospace Centre Hospital, Beijing 100049, China. [6]Department of Neurology, the First People's Hospital of Lin'an District, Zhejiang Province, Hangzhou 311399, China.

Received: 13 March 2025 Accepted: 6 May 2025
Published online: 20 May 2025

References

1. Hagen K, Linde M, Steiner TJ, Stovner LJ, Zwart JA (2012) Risk factors for medication-overuse headache: an 11-year follow-up study. The nord-trøndelag health studies. Pain 153(1):56–61. https://doi.org/10.1016/j.pain.2011.08.018
2. Schwedt TJ, Alam A, Reed ML et al (2018) Factors associated with acute medication overuse in people with migraine: results from the 2017 migraine in America symptoms and treatment (MAST) study. J Headache Pain 19(1):38. https://doi.org/10.1186/s10194-018-0865-z
3. Bigal ME, Serrano D, Buse D, Scher A, Stewart WF, Lipton RB (2008) Acute migraine medications and evolution from episodic to chronic migraine: a longitudinal population-based study. Headache 48(8):1157–1168. https://doi.org/10.1111/j.1526-4610.2008.01217.x
4. Radat F, Lanteri-Minet M (2010) What is the role of dependence-related behavior in medication-overuse headache? Headache 50(10):1597–1611. https://doi.org/10.1111/j.1526-4610.2010.01755.x
5. Corbelli I, Caproni S, Eusebi P, Sarchielli P (2012) Drug-dependence behaviour and outcome of medication-overuse headache after treatment. J Headache Pain 13(8):653–660. https://doi.org/10.1007/s10194-012-0492-z
6. Grande RB, Aaseth K, Saltyte Benth J, Gulbrandsen P, Russell MB, Lundqvist C (2009) The severity of dependence scale detects people with medication overuse: the Akershus study of chronic headache. J Neurol Neurosurg Psychiatry 80(7):784–789. https://doi.org/10.1136/jnnp.2008.168864
7. Dai W, Qiu E, Chen Y et al (2021) Enhanced functional connectivity between habenula and salience network in medication-overuse headache complicating chronic migraine positions it within the addiction disorders: an ICA-based resting-state fMRI study. J Headache Pain 22(1):107. https://doi.org/10.1186/s10194-021-01318-3
8. Chen W, Li H, Hou X, Jia X (2022) Gray matter alteration in medication overuse headache: a coordinates-based activation likelihood estimation meta-analysis. Brain Imaging Behav 16(5):2307–2319. https://doi.org/10.1007/s11682-022-00634-9
9. Mehnert J, Hebestreit J, May A (2018) Cortical and subcortical alterations in medication overuse headache. Front Neurol 9:499. https://doi.org/10.3389/fneur.2018.00499
10. Li C, Dai W, Miao S, Xie W, Yu S (2023) Medication overuse headache and substance use disorder: a comparison based on basic research and neuroimaging. Front Neurol 14:1118929. https://doi.org/10.3389/fneur.2023.1118929
11. Lai TH, Wang SJ (2018) Neuroimaging findings in patients with medication overuse headache. Curr Pain Headache Rep 22(1):1. https://doi.org/10.1007/s11916-018-0661-0
12. Edvinsson L, Grell AS, Warfvinge K (2020) Expression of the CGRP family of neuropeptides and their receptors in the trigeminal ganglion. J Mol Neurosci 70(6):930–944. https://doi.org/10.1007/s12031-020-01493-z
13. De Felice M, Ossipov MH, Wang R et al (2010) Triptan-induced enhancement of neuronal nitric oxide synthase in trigeminal ganglion dural afferents underlies increased responsiveness to potential migraine triggers. Brain 133(Pt 8):2475–2488. https://doi.org/10.1093/brain/awq159
14. Dağıdır HG, Topa E, Vuralli D, Bolay H (2023) Medication overuse headache is associated with elevated lipopolysaccharide binding protein and pro-inflammatory molecules in the bloodstream. J Headache Pain 24(1):150. https://doi.org/10.1186/s10194-023-01672-4
15. Urru M, Buonvicino D, Pistolesi A, Paccosi S, Chiarugi A (2022) Histone deacetylase inhibitors counteract CGRP signaling and pronociceptive sensitization in a rat model of medication overuse headache. J Pain 23(11):1874–1884. https://doi.org/10.1016/j.jpain.2022.05.007
16. Levine A, Liktor-Busa E, Karlage KL et al (2020) DAGLα Inhibition as a non-invasive and translational model of episodic headache. Front Pharmacol 11:615028. https://doi.org/10.3389/fphar.2020.615028
17. Kopruszinski CM, Xie JY, Eyde NM et al (2017) Prevention of stress- or nitric oxide donor-induced medication overuse headache by a calcitonin gene-related peptide antibody in rodents. Cephalalgia 37(6):560–570. https://doi.org/10.1177/0333102416650702
18. Navratilova E, Behravesh S, Oyarzo J, Dodick DW, Banerjee P, Porreca F (2020) Ubrogepant does not induce latent sensitization in a preclinical model of medication overuse headache. Cephalalgia 40(9):892–902. https://doi.org/10.1177/0333102420938652
19. Saengjaroentham C, Strother LC, Dripps I et al (2020) Differential medication overuse risk of novel anti-migraine therapeutics. Brain 143(9):2681–2688. https://doi.org/10.1093/brain/awaa211
20. Giri S, Tronvik E, Linde M, Pedersen SA, Hagen K (2023) Randomized controlled studies evaluating topiramate, botulinum toxin type A, and mABs targeting CGRP in patients with chronic migraine and medication overuse headache: a systematic review and meta-analysis. Cephalalgia 43(4):3331024231156922. https://doi.org/10.1177/03331024231156922
21. Caronna E, Gallardo VJ, Alpuente A, Torres-Ferrus M, Pozo-Rosich P (2021) Anti-CGRP monoclonal antibodies in chronic migraine with medication overuse: real-life effectiveness and predictors of response at 6 months. J Headache Pain 22(1):120. https://doi.org/10.1186/s10194-021-01328-1
22. Krymchantowski AV, Jevoux C, Krymchantowski AG, Silva-Néto RP (2023) Monoclonal antibodies for chronic migraine and medication overuse headache: a real-world study. Front Neurol 14:1129439. https://doi.org/10.3389/fneur.2023.1129439
23. Pensato U, Baraldi C, Favoni V et al (2022) Real-life assessment of erenumab in refractory chronic migraine with medication overuse headache. Neurol Sci 43(2):1273–1280. https://doi.org/10.1007/s10072-021-05426-5
24. Russo AF, Hay DL (2023) CGRP physiology, pharmacology, and therapeutic targets: migraine and beyond. Physiol Rev 103(2):1565–1644. https://doi.org/10.1152/physrev.00059.2021
25. Lundqvist C, Grande RB, Aaseth K, Russell MB (2012) Dependence scores predict prognosis of medication overuse headache: a prospective cohort from the Akershus study of chronic headache. Pain 153(3):682–686. https://doi.org/10.1016/j.pain.2011.12.008
26. Cameron C, Kelly S, Hsieh SC et al (2015) Triptans in the acute treatment of migraine: a systematic review and network meta-analysis. Headache Jul-Aug 55(Suppl 4):221–235. https://doi.org/10.1111/head.12601
27. Reagan-Shaw S, Nihal M, Ahmad N (2008) Dose translation from animal to human studies revisited. Faseb j 22(3):659–661. https://doi.org/10.1096/fj.07-9574LSF
28. Lu G, Xiao S, Meng F et al (2024) AMPK activation attenuates central sensitization in a recurrent nitroglycerin-induced chronic migraine mouse model by promoting microglial m2-type polarization. J Headache Pain 25(1):29. https://doi.org/10.1186/s10194-024-01739-w
29. Burgos-Vega CC, Quigley LD, Trevisan Santos Dos G et al (2019) Non-invasive dural stimulation in mice: a novel preclinical model of migraine. Cephalalgia 39(1):123–134. https://doi.org/10.1177/0333102418779557
30. Fried NT, Maxwell CR, Elliott MB, Oshinsky ML (2018) Region-specific disruption of the blood-brain barrier following repeated inflammatory dural stimulation in a rat model of chronic trigeminal allodynia. Cephalalgia 38(4):674–689. https://doi.org/10.1177/0333102417703764
31. Li C, Li Y, Zhang W, Ma Z, Xiao S, Xie W, Miao S, Li B, Lu G, Liu Y, Bai W, Yu S (2023) Dopaminergic Projections from the Hypothalamic A11 Nucleus to the Spinal Trigeminal Nucleus Are Involved in Bidirectional Migraine Modulation. Int J Mol Sci 24(23):16876. https://doi.org/10.3390/ijms242316876 PMID: 38069205
32. Chaplan SR, Bach FW, Pogrel JW, Chung JM, Yaksh TL (1994) Quantitative assessment of tactile allodynia in the rat paw. J Neurosci Methods 53(1):55–63. https://doi.org/10.1016/0165-0270(94)90144-9
33. Christensen SL, Hansen RB, Storm MA et al (2020) Von frey testing revisited: provision of an online algorithm for improved accuracy of 50% thresholds. Eur J Pain 24(4):783–790. https://doi.org/10.1002/ejp.1528
34. Zhang L, Lu C, Kang L et al (2022) Temporal characteristics of astrocytic activation in the TNC in a mice model of pain induced by recurrent dural infusion of inflammatory soup. J Headache Pain 23(1):8. https://doi.org/10.1186/s10194-021-01382-9
35. Bonnet C, Hao J, Osorio N et al (2019) Maladaptive activation of Nav1.9 channels by nitric oxide causes triptan-induced medication overuse headache. Nat Commun 10(1):4253. https://doi.org/10.1038/s41467-019-12197-3
36. Li S, Liao Y, Dong Y et al (2021) Microglial deletion and inhibition alleviate behavior of post-traumatic stress disorder in mice. J Neuroinflammation 18(1):7. https://doi.org/10.1186/s12974-020-02069-9
37. Xiao S, Lu G, Liu J et al (2024) Brain-wide mapping of c-Fos expression in nitroglycerin-induced models of migraine. J Headache Pain 25(1):136. https://doi.org/10.1186/s10194-024-01837-9

38. Lim CJM, Platt B, Janhunen SK, Riedel G (2023) Comparison of automated video tracking systems in the open field test: ANY-Maze versus EthoVision XT. J Neurosci Methods 397:109940. https://doi.org/10.1016/j.jneumeth.2023.109940
39. Yuan H, Na W, Li B et al (2025) Optogenetic cortical spreading depression originating from the primary visual cortex induces migraine-like pain and anxiety behaviors in freely moving C57BL/6 J mice. J Headache Pain 26(1):44. https://doi.org/10.1186/s10194-025-01983-8
40. Yang C, Gong Z, Zhang X et al (2023) Neuropeptide Y in the medial habenula alleviates migraine-like behaviors through the Y1 receptor. J Headache Pain 24(1):61. https://doi.org/10.1186/s10194-023-01596-z
41. Hu Y, Du W, Qi J, et al (2024) Comparative brain-wide mapping of ketamine- and isoflurane-activated nuclei and functional networks in the mouse brain. Elife 12:RP88420. https://doi.org/10.7554/eLife.88420
42. Sciarra C, Chiarotti G, Laio F, Ridolfi L (2018) A change of perspective in network centrality. Sci Rep 8(1):15269. https://doi.org/10.1038/s41598-018-33336-8
43. Rubinov M, Sporns O (2010) Complex network measures of brain connectivity: uses and interpretations. Neuroimage 52(3):1059–1069. https://doi.org/10.1016/j.neuroimage.2009.10.003
44. Shannon P, Markiel A, Ozier O et al (2003) Cytoscape: a software environment for integrated models of biomolecular interaction networks. Genome Res 13(11):2498–2504. https://doi.org/10.1101/gr.1239303
45. Bertz R, Bhardwaj R, Morris BA, Ashbrenner E, Coric V, Croop R (2023) A placebo-controlled, randomized, single and multiple dose study to evaluate the safety, tolerability, and pharmacokinetics of rimegepant in healthy participants. Cephalalgia 43(6):3331024231179131. https://doi.org/10.1177/03331024231179131
46. Zheng N, Zeng J, Ji QC et al (2014) Improved liquid-liquid extraction with inter-well volume replacement dilution workflow and its application to quantify BMS-927711 in rat dried blood spots by UHPLC-MS/MS. J Pharm Biomed Anal 89:240–250. https://doi.org/10.1016/j.jpba.2013.11.017
47. Mulder IA, Li M, de Vries T et al (2020) Anti-migraine calcitonin gene-related peptide receptor antagonists worsen cerebral ischemic outcome in mice. Ann Neurol 88(4):771–784. https://doi.org/10.1002/ana.25831
48. Burstein R, Cutrer MF, Yarnitsky D (2000) The development of cutaneous allodynia during a migraine attack clinical evidence for the sequential recruitment of spinal and supraspinal nociceptive neurons in migraine. Brain 123(Pt 8):1703–1709. https://doi.org/10.1093/brain/123.8.1703
49. Bigal ME, Ashina S, Burstein R et al (2008) Prevalence and characteristics of allodynia in headache sufferers: a population study. Neurology 70(17):1525–1533. https://doi.org/10.1212/01.wnl.0000310645.31020.b1
50. Lipton RB, Bigal ME, Ashina S et al (2008) Cutaneous allodynia in the migraine population. Ann Neurol 63(2):148–158. https://doi.org/10.1002/ana.21211
51. Dodick D, Freitag F (2006) Evidence-based understanding of medication-overuse headache: clinical implications. Headache 46(Suppl 4):S202–S211. https://doi.org/10.1111/j.1526-4610.2006.00604.x
52. Sebastianelli G, Casillo F, Abagnale C et al (2023) Central sensitization mechanisms in chronic migraine with medication overuse headache: a study of thalamocortical activation and lateral cortical inhibition. Cephalalgia 43(10):3331024231202240. https://doi.org/10.1177/03331024231202240
53. Wang Y, Dong L, Zhang Y et al (2023) Activation of the microglial P2X7R/NLRP3 inflammasome mediates central sensitization in a mouse model of medication overuse headache. Front Mol Neurosci 16:1177171. https://doi.org/10.3389/fnmol.2023.1177171
54. Ashina S, Terwindt GM, Steiner TJ et al (2023) Medication overuse headache. Nat Rev Dis Primers 9(1):5. https://doi.org/10.1038/s41572-022-00415-0
55. Gong Z, Yang C, Dai W et al (2023) Annexin A1 exerts analgesic effect in a mouse model of medication overuse headache. iScience 26(11):108153. https://doi.org/10.1016/j.isci.2023.108153
56. Ryu S, Zhang J, Simoes R et al (2024) Regulatory T cells require peripheral CCL2-CCR2 signaling to facilitate the resolution of medication overuse headache-related behavioral sensitization. J Headache Pain 25(1):197. https://doi.org/10.1186/s10194-024-01900-5
57. Guzman G, Kopruszinski CM, Barber KR et al (2025) Chronification of migraine sensitizes to CGRP in male and female mice. Cephalalgia 45(2):3331024251317446. https://doi.org/10.1177/03331024251317446
58. Terem A, Fatal Y, Peretz-Rivlin N et al (2023) Claustral neurons projecting to frontal cortex restrict opioid consumption. Curr Biol 33(13):2761-2773.e8. https://doi.org/10.1016/j.cub.2023.05.065
59. Takahashi TT, Ornello R, Quatrosi G et al (2021) Medication overuse and drug addiction: a narrative review from addiction perspective. J Headache Pain 22(1):32. https://doi.org/10.1186/s10194-021-01224-8
60. Louter MA, Bosker JE, van Oosterhout WP et al (2013) Cutaneous allodynia as a predictor of migraine chronification. Brain 136(Pt 11):3489–3496. https://doi.org/10.1093/brain/awt251
61. Camarini R, Pautassi RM (2016) Behavioral sensitization to ethanol: neural basis and factors that influence its acquisition and expression. Brain Res Bull 125:53–78. https://doi.org/10.1016/j.brainresbull.2016.04.006
62. Strakowski SM, Sax KW, Setters MJ, Keck PE Jr (1996) Enhanced response to repeated d-amphetamine challenge: evidence for behavioral sensitization in humans. Biol Psychiatry 40(9):872–880. https://doi.org/10.1016/0006-3223(95)00497-1
63. Robinson TE, Berridge KC (2008) Review, the incentive sensitization theory of addiction: some current issues. Philos Trans R Soc Lond B Biol Sci 363(1507):3137–46. https://doi.org/10.1098/rstb.2008.0093
64. Kalivas PW, Duffy P (1988) Effects of daily cocaine and morphine treatment on somatodendritic and terminal field dopamine release. J Neurochem 50(5):1498–1504. https://doi.org/10.1111/j.1471-4159.1988.tb03036.x
65. Kuczenski R, Segal D (1989) Concomitant characterization of behavioral and striatal neurotransmitter response to amphetamine using in vivo microdialysis. J Neurosci 9(6):2051–2065. https://doi.org/10.1523/jneurosci.09-06-02051.1989
66. Volkow ND, Wang GJ, Telang F et al (2006) Cocaine cues and dopamine in dorsal striatum: mechanism of craving in cocaine addiction. J Neurosci 26(24):6583–6588. https://doi.org/10.1523/jneurosci.1544-06.2006
67. Berridge KC, Robinson TE (2016) Liking, wanting, and the incentive-sensitization theory of addiction. Am Psychol 71(8):670–679. https://doi.org/10.1037/amp0000059
68. Cupini LM, De Murtas M, Costa C et al (2009) Obsessive-compulsive disorder and migraine with medication-overuse headache. Headache 49(7):1005–1013. https://doi.org/10.1111/j.1526-4610.2009.01457.x
69. Radat F, Creac'h C, Swendsen JD et al (2005) Psychiatric comorbidity in the evolution from migraine to medication overuse headache. Cephalalgia 25(7):519–522. https://doi.org/10.1111/j.1468-2982.2005.00910.x
70. Bigal ME, Lipton RB (2009) Overuse of acute migraine medications and migraine chronification. Curr Pain Headache Rep 13(4):301–307. https://doi.org/10.1007/s11916-009-0048-3
71. Atasoy HT, Atasoy N, Unal AE, Emre U, Sumer M (2005) Psychiatric comorbidity in medication overuse headache patients with pre-existing headache type of episodic tension-type headache. Eur J Pain 9(3):285–291. https://doi.org/10.1016/j.ejpain.2004.07.006
72. Zwart J-A, Dyb G, Hagen K, Svebak S, Stovner LJ, Holmen J (2004) Analgesic overuse among subjects with headache, neck, and low-back pain. Neurology 62(9):1540–1544. https://doi.org/10.1212/01.WNL.0000123262.96132.FC
73. Monteith TS, Oshinsky ML (2009) Tension-type headache with medication overuse: pathophysiology and clinical implications. Curr Pain Headache Rep 13(6):463–469. https://doi.org/10.1007/s11916-009-0075-0
74. Ashina M, Hansen JM, Do TP, Melo-Carrillo A, Burstein R, Moskowitz MA (2019) Migraine and the trigeminovascular system-40 years and counting. Lancet Neurol 18(8):795–804. https://doi.org/10.1016/s1474-4422(19)30185-1
75. Burstein R, Jakubowski M, Garcia-Nicas E et al (2010) Thalamic sensitization transforms localized pain into widespread allodynia. Ann Neurol 68(1):81–91. https://doi.org/10.1002/ana.21994
76. Goldstein RZ, Volkow ND (2002) Drug addiction and its underlying neurobiological basis: neuroimaging evidence for the involvement of the frontal cortex. Am J Psychiatry 159(10):1642–1652. https://doi.org/10.1176/appi.ajp.159.10.1642
77. Kwon J, Kim HJ, Lee HR, Ho WK, Kim JH, Lee SH (2023) Rewiring of prelimbic inputs to the nucleus accumbens core underlies

cocaine-induced behavioral sensitization. Biol Psychiatry 94(5):378–392. https://doi.org/10.1016/j.biopsych.2022.12.024
78. Chen Z, Tang S, Xiao X et al (2024) Adiponectin receptor 1-mediated basolateral amygdala-prelimbic cortex circuit regulates methamphetamine-associated memory. Cell Rep 43(12):115074. https://doi.org/10.1016/j.celrep.2024.115074
79. Martínez-Rivera FJ, Pérez-Torres J, Velázquez-Díaz CD et al (2023) A novel insular/orbital-prelimbic circuit that prevents persistent avoidance in a rodent model of compulsive behavior. Biol Psychiatry 93(11):1000–1009. https://doi.org/10.1016/j.biopsych.2022.02.008
80. Fu S, Sun H, Wang J et al (2024) Impaired neuronal macroautophagy in the prelimbic cortex contributes to comorbid anxiety-like behaviors in rats with chronic neuropathic pain. Autophagy 20(7):1559–1576. https://doi.org/10.1080/15548627.2024.2330038
81. Liu Y, Li A, Bair-Marshall C et al (2023) Oxytocin promotes prefrontal population activity via the PVN-PFC pathway to regulate pain. Neuron 111(11):1795-1811.e7. https://doi.org/10.1016/j.neuron.2023.03.014
82. Jia Z, Tang W, Zhao D, Yu S (2017) Disrupted functional connectivity between the periaqueductal gray and other brain regions in a rat model of recurrent headache. Sci Rep 7(1):3960. https://doi.org/10.1038/s41598-017-04060-6
83. Stujenske JM, O'Neill PK, Fernandes-Henriques C et al (2022) Prelimbic cortex drives discrimination of non-aversion via amygdala somatostatin interneurons. Neuron 110(14):2258-2267.e11. https://doi.org/10.1016/j.neuron.2022.03.020
84. Wu GY, Zheng XX, Zhao SL et al (2023) The prelimbic cortex regulates itch processing by controlling attentional bias. iScience 26(1):105829. https://doi.org/10.1016/j.isci.2022.105829
85. Ji G, Sun H, Fu Y et al (2010) Cognitive impairment in pain through amygdala-driven prefrontal cortical deactivation. J Neurosci 30(15):5451–5464. https://doi.org/10.1523/jneurosci.0225-10.2010
86. DeNardo LA, Liu CD, Allen WE et al (2019) Temporal evolution of cortical ensembles promoting remote memory retrieval. Nat Neurosci 22(3):460–469. https://doi.org/10.1038/s41593-018-0318-7
87. Huang WC, Zucca A, Levy J, Page DT (2020) Social behavior is modulated by valence-encoding mpfc-amygdala sub-circuitry. Cell Rep 32(2):107899
88. Niddam DM, Wu SW, Lai KL, Yang YY, Wang YF, Wang SJ (2023) An altered reward system characterizes chronic migraine with medication overuse headache. Cephalalgia 43(4):3331024231158088. https://doi.org/10.1177/03331024231158088
89. Balleine BW (2011) Sensation, Incentive Learning, and the Motivational Control of Goal-Directed Action. In: Gottfried JA, ed. Neurobiology of Sensation and Reward. CRC Press/Taylor & Francis.Copyright © 2011 by Taylor and Francis Group, LLC
90. Swanson AM, DePoy LM, Gourley SL (2017) Inhibiting Rho kinase promotes goal-directed decision making and blocks habitual responding for cocaine. Nat Commun 8(1):1861. https://doi.org/10.1038/s41467-017-01915-4
91. Chen BT, Yau HJ, Hatch C et al (2013) Rescuing cocaine-induced prefrontal cortex hypoactivity prevents compulsive cocaine seeking. Nature 496(7445):359–362. https://doi.org/10.1038/nature12024
92. Volkow ND, Wise RA, Baler R (2017) The dopamine motive system: implications for drug and food addiction. Nat Rev Neurosci 18(12):741–752. https://doi.org/10.1038/nrn.2017.130
93. Hernández-Ortiz E, Luis-Islas J, Tecuapetla F, Gutierrez R, Bermúdez-Rattoni F (2023) Top-down circuitry from the anterior insular cortex to VTA dopamine neurons modulates reward-related memory. Cell Rep 42(11):113365. https://doi.org/10.1016/j.celrep.2023.113365
94. Sun K, Mu Q, Chang H et al (2020) Postretrieval microinjection of baclofen into the agranular insular cortex inhibits morphine-induced CPP by disrupting reconsolidation. Front Pharmacol 11:743. https://doi.org/10.3389/fphar.2020.00743
95. Edvinsson L, Haanes KA, Warfvinge K, Krause DN (2018) CGRP as the target of new migraine therapies - successful translation from bench to clinic. Nat Rev Neurol 14(6):338–350. https://doi.org/10.1038/s41582-018-0003-1
96. Russo AF (2015) Calcitonin gene-related peptide (CGRP): a new target for migraine. Annu Rev Pharmacol Toxicol 55:533–552. https://doi.org/10.1146/annurev-pharmtox-010814-124701
97. Croop R, Lipton RB, Kudrow D et al (2021) Oral rimegepant for preventive treatment of migraine: a phase 2/3, randomised, double-blind, placebo-controlled trial. Lancet 397(10268):51–60. https://doi.org/10.1016/s0140-6736(20)32544-7
98. Yu S, Kim BK, Guo A et al (2023) Safety and efficacy of rimegepant orally disintegrating tablet for the acute treatment of migraine in China and South Korea: a phase 3, double-blind, randomised, placebo-controlled trial. Lancet Neurol 22(6):476–484. https://doi.org/10.1016/s1474-4422(23)00126-6
99. Tepper SJ, Diener HC, Ashina M et al (2019) Erenumab in chronic migraine with medication overuse: subgroup analysis of a randomized trial. Neurology 92(20):e2309–e2320. https://doi.org/10.1212/wnl.0000000000007497
100. Goadsby PJ, Reuter U, Hallström Y et al (2017) A controlled trial of erenumab for episodic migraine. N Engl J Med 377(22):2123–2132. https://doi.org/10.1056/NEJMoa1705848
101. Ahn AH, Basbaum AI (2005) Where do triptans act in the treatment of migraine? Pain 115(1–2):1–4. https://doi.org/10.1016/j.pain.2005.03.008
102. Blair HA (2023) Rimegepant: A review in the acute treatment and preventive treatment of migraine. CNS Drugs 37(3):255–265. https://doi.org/10.1007/s40263-023-00988-8
103. Warfvinge K, Edvinsson L (2019) Distribution of CGRP and CGRP receptor components in the rat brain. Cephalalgia 39(3):342–353. https://doi.org/10.1177/0333102417728873
104. Sexton PM (1991) Central nervous system binding sites for calcitonin and calcitonin gene-related peptide. Mol Neurobiol 5(2–4):251–273. https://doi.org/10.1007/bf02935550
105. Feistel S, Albrecht S, Messlinger K (2013) The calcitonin gene-related peptide receptor antagonist MK-8825 decreases spinal trigeminal activity during nitroglycerin infusion. J Headache Pain 14(1):93. https://doi.org/10.1186/1129-2377-14-93
106. Hostetler ED, Joshi AD, Sanabria-Bohórquez S et al (2013) In vivo quantification of calcitonin gene-related peptide receptor occupancy by telcagepant in rhesus monkey and human brain using the positron emission tomography tracer [11C]MK-4232. J Pharmacol Exp Ther 347(2):478–486. https://doi.org/10.1124/jpet.113.206458

Publisher's Note